

Научном већу

Института за физику

Прегревица 118, Земун

Предмет: Реизбор у звање истраживач сарадник

Молим Научно веће Института за физику да покрене поступак за мој реизбор у звање истраживач сарадник.

Прилажем:

- Молба за реизбор у звање
- Биографију
- Списак и фотокопије научних радова
- Преглед научне активности
- Мишљење руководиоца пројекта
- Потврду о упису на докторске академске студије
- Фотокопију дипломе

С поштовањем, Иван Радојичић

Београд, 21.05.2018.

МИШЉЕЊЕ РУКОВОДИОЦА ПРОЈЕКТА

Иван Радојичић, дипл. Физичар, је ангажован на пројекту III45016, где се бави истраживањима која су везана за интеракцију ласерског зрачења са парама калијума и рубидијума. У оквиру досадашњих истраживања објавио је два научни рад из категорија М21, као и једно саопштење са међународног скупа у целости из категорије М34. С обзиром на све изложено, предлажем Нучном већу Института за Физику да Ивана Радојичића поново изабере у звање истраживач-сарадник.

Предлажем комисију за избор у звање у следећем саставу:

Проф. др Бранислав Јеленковић, научни саветник Института за физику

др Дејан Пантелић, научни саветник Института за физику

Др Милорад Кураица, редовни професор, Физички факултет

Проф. др Бранислав Јеленковић, научни саветник

Руководилац пројекта



Биографија кандидата

Иван Радојичић је рођен у Чачку, Република Србија, 09.07.1980. године. У Ужицу је завршио основну школу и Гимназију, природно – математички смер. 2010. године дипломира (основне академске студије) на Физичком факултету, Универзитета у Београду, смер Примењена физика и информатика са просечном оценом 8,68. Дипломски рад је одбранио на тему „Конструкција диодног ласера са спољашњим резонатором и стабилизација таласне дужине емитовања на хиперфини прелаз рубидијума“. Од 01.01. 2011. године је запослен у Институту за физику, са ангажовањем на пројекту Министарства просвете, науке и технолошког развоја "Генерисање и карактеризација нанофотонских функционалних структура у биомедицини и информатици". Од јануара 2012. године је уписан на Докторске академске студије Физичког факултета Универзитета у Београду, смер Квантна оптика и ласери . До сада је публикувао два научна рада у часописима категорије (M21), једно саопштење са међународног скупа штампано у целини (M33), седам саопштење са међународног скупа штампано у изводу (M34) и три саопштења са скупа националног значаја штампано у изводу (M64).

Списак радова:

M21:

M Gharavipour, C Affolderbach, F Gruet, I S Radojičić, A J Krmpot, B M Jelenković, G Mileti, Optically-detected spin-echo method for relaxation times measurements in a Rb atomic vapor, *New Journal of Physics*, 19, 10.1088/1367-2630/aa73c2, Jun2017.

Ivan S. Radojičić, Milan Radonjić, Marina M. Lekić, Zoran D. Grujić, Dragan Lukić, Branislav Jelenković, Raman-Ramsey electromagnetically induced transparency in the configuration of counterpropagating pump and probe in vacuum Rb cell, *Journal of the Optical Society of America B: Optical Physics*, *Optical Society of America*, 32, 3, pp. 426 - 430, 0740-3224, 10.1364/JOSAB.32.000426, 2015.

M33:

Bojan Zlatković, Aleksandar Krmpot, Ivan Radojičić, Dušan Arsenović, Milan Minić, Branislav Jelenković, Slow and Stored Light in Amplifying Four Way Mixing Process, 2016 18th International Conference on Transparent Optical Networks (ICTON), IEEE, x, pp. 1 - 3, ISSN: 2161-2064, 10.1109/ICTON.2016.7550577, Италија, 10. - 14. Jul, 2016

PAPER • OPEN ACCESS

Optically-detected spin-echo method for relaxation times measurements in a Rb atomic vapor

To cite this article: M Gharavipour *et al* 2017 *New J. Phys.* **19** 063027

View the [article online](#) for updates and enhancements.

Related content

- [Metrological characterization of the pulsed Rb clock with optical detection](#)
S Micalizio, C E Calosso, A Godone et al.
- [Transient development of Zeeman electromagnetically induced transparency during propagation of Raman–Ramsey pulses through Rb buffer gas cell](#)
S N Nikoli, M Radonji, N M Lui et al.
- [Double-resonance lineshapes in a cell with wall coating and buffer gas¹](#)
Svenja Knappe and Hugh G Robinson



PAPER

Optically-detected spin-echo method for relaxation times measurements in a Rb atomic vapor

OPEN ACCESS

RECEIVED

21 December 2016

REVISED

18 April 2017

ACCEPTED FOR PUBLICATION

17 May 2017

PUBLISHED

26 June 2017

Original content from this work may be used under the terms of the [Creative Commons Attribution 3.0 licence](#).

Any further distribution of this work must maintain attribution to the author(s) and the title of the work, journal citation and DOI.

M Gharavipour^{1,3}, C Affolderbach¹, F Gruet¹, I S Radojičić², A J Krmpot², B M Jelenković² and G Mileti^{1,3}¹ Laboratoire Temps-Fréquence (LTF), Institut de Physique, Université de Neuchâtel, Neuchâtel CH-2000, Switzerland² Institute of Physics Belgrade, University of Belgrade, Pregrevice 118, 11080 Belgrade, Serbia³ Authors to whom any correspondence should be addressedE-mail: mohammadreza.gharavipour@unine.ch and gaetano.mileti@unine.ch

Keywords: relaxation times, vapor cell atomic clock, spin-echo, optical detection, Ramsey scheme

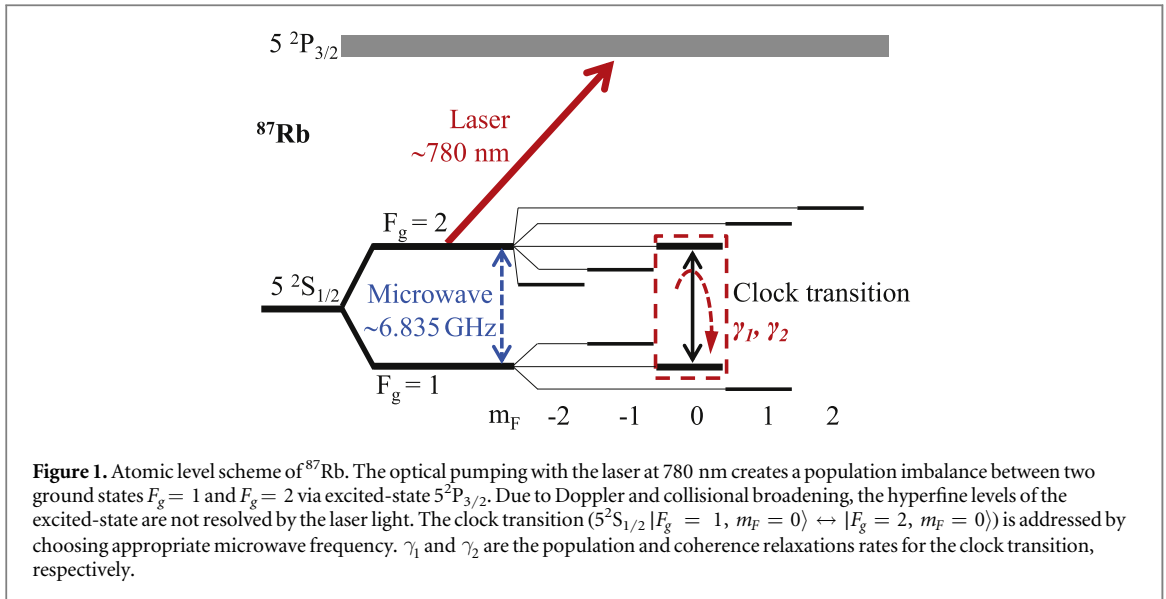
Abstract

We introduce and demonstrate an experimental method, optically-detected spin-echo (ODSE), to measure ground-state relaxation times of a rubidium (Rb) atomic vapor held in a glass cell with buffer-gas. The work is motivated by our studies on high-performance Rb atomic clocks, where both population and coherence relaxation times (T_1 and T_2 , respectively) of the ‘clock transition’ ($5^2S_{1/2} |F_g = 1, m_F = 0\rangle \leftrightarrow |F_g = 2, m_F = 0\rangle$) are relevant. Our ODSE method is inspired by classical nuclear magnetic resonance spin-echo method, combined with optical detection. In contrast to other existing methods, like continuous-wave double-resonance (CW-DR) and Ramsey-DR, principles of the ODSE method allow suppression of decoherence arising from the inhomogeneity of the static magnetic field across the vapor cell, thus enabling measurements of intrinsic relaxation rates, as properties of the cell alone. Our experimental result for the coherence relaxation time, specific for the clock transition, measured with the ODSE method is in good agreement with the theoretical prediction, and the ODSE results are validated by comparison to those obtained with Franzen, CW-DR and Ramsey-DR methods. The method is of interest for a wide variety of quantum optics experiments with optical signal readout.

1. Introduction

Alkali atomic vapors are widely used in many types of high-resolution atomic physics experiments like nuclear magnetic resonance (NMR) [1] and precision measurements in applications such as optical magnetometry [2], vapor cell atomic frequency standards [3, 4], quantum entanglement and information storage [5], miniature atomic clocks [6], navigation systems [7–9], spin squeezing [10]. All these applications rely on long-lived ground-state spin-polarization of the alkali vapor in the cell [11]. Particularly in the vapor-cell atomic clocks, the clock stability critically depends on width and contrast of the atomic resonance line. The resonance linewidth is determined by various parameters, and ultimately, by the relaxation processes occurring in the cell. Like in NMR, alkali atoms in the vapor cell may lose their polarization due to various types of collisions, interactions with electro-magnetic fields, and also due to inhomogeneity of the static magnetic field.

Studies of relaxation processes in various spin-polarized systems have a long-standing history of more than 70 years. In the case of atomic relaxations in alkali vapors, Franzen presented the ‘relaxation in the dark’ method [12] in 1959 and measured the population relaxation time of optically-pumped Rb atoms in the vapor cell. Franzen’s method has been modified and used by other groups to determine both population and coherence relaxation times in Rb or Cs wall-coated vapor cells [13–16]. Moreover, methods of nonlinear magneto-optical rotation [11, 17], ground-state Hanle effect [18, 19] and optically detected magnetic resonance [19, 20] were employed to measure the hyperfine and the Zeeman relaxation times in wall-coated or in buffer-gas alkali vapor cells. Various modified NMR spin-echo techniques [21] have been studied both theoretically and experimentally for solid-state systems to extend the coherence time [22, 23]. Similar techniques like dynamical decoupling approach [24, 25] and gradient echo memory [26] applied in quantum memory studies aim for example to



minimize the detrimental effect of inhomogeneous broadening on the coherence storage time of the quantum bit (qubit) or to use the artificially created broadening for storage of broad-band optical pulses without deterioration of the storage time [27–29].

In this paper, we present our ‘optically-detected spin-echo’ (ODSE) method to measure the relaxation times in a Rb vapor cell with buffer-gas. This method is a combination of Franzen [12], Ramsey-DR [16] and NMR spin-echo [21] techniques. We apply the ODSE method to our high-performance ^{87}Rb atomic frequency-standard setup presented in [30, 31] and show how to determine the intrinsic coherence relaxation time (T_2) specifically for the ‘clock transition’ ($5^2\text{S}_{1/2} |F_g = 1, m_F = 0\rangle \leftrightarrow |F_g = 2, m_F = 0\rangle$), see figure 1). Here we use the term ‘intrinsic’ to describe the relaxations that do not include any influence of any electro-magnetic field but are influenced only by the various types of collisions that depend on the cell design and the temperature [19] (see section 2). Gradients in the static magnetic field across the vapor cell are some of the main sources of the relaxation processes. Such induced relaxation processes may mask the real intrinsic relaxation times during measurements, thus hindering their precise determination. The ODSE method enables measurements that are free of the influence of the static magnetic field gradients.

In section 2 we briefly recall the theory of relaxation processes in a buffer-gas vapor cell [3], and use it to estimate the ‘intrinsic’ population and coherence relaxation times (T_1 and T_2 respectively) of the clock transition in our ^{87}Rb vapor cell. In section 3, we introduce the experimental setup which is basically a Rb atomic clock [30, 31]. Finally in section 4, we present the results of relaxation times measured in the same ^{87}Rb vapor cell by using ODSE, Franzen, continuous-wave double-resonance (CW-DR), and Ramsey-DR methods. The advantages and limitations of these methods are discussed.

2. Theory of relaxation processes in a buffer-gas vapor cell

Ultra-narrow signal linewidths employed in atomic precision experiments and instrumentations, such as atomic clocks, are ultimately limited by the relaxation processes in the atomic sample. For example in a Rb atomic clock, the frequency of a quartz oscillator is stabilized to the frequency of the ^{87}Rb hyperfine clock transition [32] observed in a Rb vapor cell. Rb atoms are optically pumped with a laser to create a population imbalance and microwave interrogation creates a coherence between the two ground states $F_g = 1$ and $F_g = 2$ of ^{87}Rb atoms. Due to the relaxation processes, this population imbalance and coherence may be destroyed and the prepared Rb atoms lose their polarization. The dynamics of this process is characterized by the relaxation times on the atomic levels. The two parameters of longitudinal relaxation rate γ_1 and transverse relaxation rate γ_2 —which are inverse of the relaxation times T_1 and T_2 , respectively—describe the population and coherence relaxations for the clock transition, respectively (see figure 1).

We use the well-known relaxation theory [3] and the experimentally-determined parameters presented in [3] to estimate approximately γ_1 and γ_2 for our ^{87}Rb vapor cell. Collisions of polarized ^{87}Rb atoms with the cell walls, with buffer-gas particles and with other Rb atoms—the latter is known as spin-exchange—are the sources of relaxation processes occurring in a vapor cell. The total intrinsic population and coherence relaxation rates, γ_i (here and in the following index i stands for 1 and 2 for the population and coherence, respectively), are equal to

Table 1. Calculated intrinsic relaxation rates/times in Rb vapor cell, at $T = 336$ K.

	γ_1 (s ⁻¹)	γ_2 (s ⁻¹)
Buffer gas collisions (γ_{iBG})	12	79
Diffusion to cell walls (γ_{iW})	26	25
Spin-exchange (γ_{iSE})	185	116
Total rates	223	220
Calculated relaxation times (ms)	$T_1 = 4.5$ (3)	$T_2 = 4.5$ (3)

the sum of the three relaxation processes induced by the cell walls γ_{iW} , the buffer-gas γ_{iBG} and spin-exchange γ_{iSE} .

The presence of a buffer gas in the cell reduces the rate of depolarizing collisions between Rb atoms and the cell walls. Therefore, relaxation rates γ_{iW} , due to collisions of Rb atoms with the cell-walls, depend on the cell dimensions, cell temperature T and the total buffer-gas pressure, P , in the cell. In lowest order diffusion approximation, it is described by [3]:

$$\gamma_{iW} = ((2.405/a)^2 + (\pi/L)^2)D_i(P_0/P), \quad (1)$$

where $a = 1.25$ cm and $L = 2.5$ cm are the radius and length of our cylindrical ⁸⁷Rb vapor cell, respectively. D_i is the diffusion constant of Rb atoms in the buffer-gas particles of interest which is proportional to $T^{3/2}$, P_0 is the standard atmospheric pressure (1013.25 mbar) and P is about 33 mbar in our vapor cell.

Rb atoms also collide with the buffer-gas molecules in the vapor cell, which changes the electron density at the Rb nucleus and results in a change of hyperfine coupling in the Rb atoms [33]. The resulting buffer-gas relaxation rate γ_{iBG} is described as:

$$\gamma_{iBG} = L_0 \bar{v}_r \sigma_i (P/P_0), \quad (2)$$

where $L_0 = 2.686\,7774(47) \times 10^{25} \text{ m}^{-3}$ at 0 °C is Loschmidt's constant, \bar{v}_r is the mean relative velocity between a ⁸⁷Rb atom and a buffer-gas particle, and σ_i are the collisional cross-sections between colliding particles responsible for population and coherence relaxations. The temperature dependence of the above equation appears in the average relative velocity $\bar{v}_r = (8k_B T/\pi\mu)^{1/2}$ where k_B is the Boltzmann constant and μ is the reduced mass of the colliding particles (here Rb and buffer-gas atoms).

Note that in the case of anti-relaxation wall-coated cells the relaxation processes as described by equations (1) and (2) do not apply and the relaxation rates are instead governed by the properties and the quality (such as purity and coverage) of the coating [34–36]. Such wall-coated cells are however not considered in this study.

Collisions between Rb atoms in the vapor cell result in de-coherence due to spin exchange. The resulting population γ_{1SE} and coherence γ_{2SE} broadening are described by:

$$\gamma_{1SE} = n \bar{v}_s \sigma_{SE}, \quad (3)$$

$$\gamma_{2SE} = \gamma_{1SE}(6I + 1)/(8I + 4), \quad (4)$$

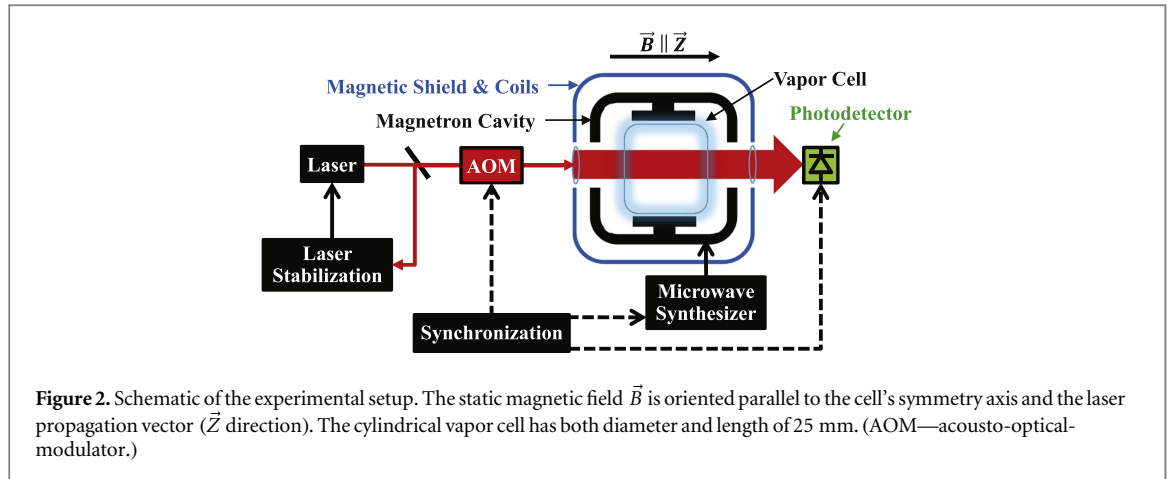
respectively, where n is the number density of the Rb vapor, \bar{v}_s is the average relative velocity between two ⁸⁷Rb atoms and $\sigma_{SE} = 1.6 \times 10^{-18} \text{ m}^2$ is the spin-exchange cross section. I is the nuclear spin and for ⁸⁷Rb is equal to 3/2.

The total expected relaxation rates in our cell are given by:

$$\gamma_i = \gamma_{iBG} + \gamma_{iW} + \gamma_{iSE}. \quad (5)$$

All these contributions to the intrinsic population and coherence relaxation rates are listed in table 1. They were calculated from equations (1)–(4) for the clock transition in our ⁸⁷Rb vapor cell using experimentally measured parameters for D_i and σ_i taken from [3]. Finally, both intrinsic relaxation times for the clock transition are calculated to be $T_1 \approx T_2 = 4.5$ ms. We note that the reported literature values for D_i and σ_i show considerable scatter, which results in a total uncertainty of 7% for both intrinsic T_1 and T_2 [12, 37–39].

In addition to the various presented types of collisions of the polarized Rb atoms in the vapor cell, their interactions with other electromagnetic fields may also be interpreted as sources of relaxations. The electromagnetic fields present in our atomic clock are the optical and the microwave fields that are used to prepare, drive and detect the resonance [30, 32] and the static magnetic field applied to lift the Zeeman degeneracy. The latter may have some residual inhomogeneity across the vapor cell. In a microscopic view, Rb atoms can move in the vapor cell and—due to the field inhomogeneity—they may experience various static magnetic fields. This effect introduces additional dephasing [40] which results in a decrease of the measured



coherence relaxation time depending on the method (see section 4). In NMR, the overall coherence relaxation time T_2^* due to the field inhomogeneity is given by [41]:

$$T_2^{*-1} = T_2^{-1} + \eta G^2, \quad (6)$$

where, T_2 is the intrinsic coherence relaxation time, G is the local gradient of the static magnetic field and η is a proportionality factor depending on atomic and experimental parameters.

In this study, we determine the coherence time T_2^* by using CW-DR and Ramsey-DR schemes (sections 4.2 and 4.3, respectively), while with ODSE method the intrinsic coherence relaxation time T_2 is obtained (section 4.4).

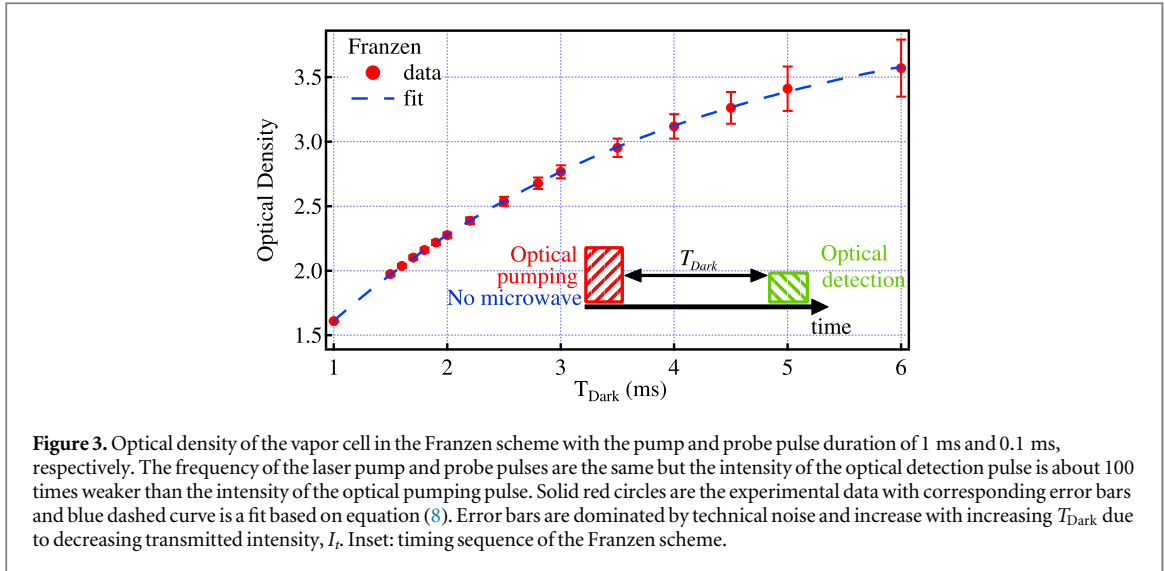
The system studied here is an alkali vapor cell with relatively high buffer-gas pressure, where the Rb atoms are effectively localized to a few micrometers over the measurement timescales. Due to this localization, the sample shows inhomogeneous shifts and broadenings because of the inhomogeneity of external fields [42]. This is fundamentally different from the case of anti-relaxation wall-coated cells without buffer gas where the atoms move freely through the entire cell volume and experience only homogeneous shifts and broadenings as well as narrowing [43].

3. Experimental setup

Figure 2 shows the schematics of our experimental setup, basically a Rb atomic clock, whose details were previously presented in [30, 31]. It consists of three main parts: (1) the physics package containing the microwave cavity and the vapor cell, (2) the compact frequency-stabilized laser head (LH), and (3) the microwave synthesizer. The physics package contains the in-house-made cylindrical glass cell with both diameter and length of 25 mm. The cell contains isotopically enriched ^{87}Rb and a mixture of Argon and Nitrogen as buffer gases. The vapor cell is placed in a compact magnetron-type microwave cavity which resonates at the ^{87}Rb clock transition frequency of ≈ 6.835 GHz, with a TE_{011} -like field-mode geometry [44]. A magnetic coil placed around the cavity generates a static magnetic field oriented parallel to the cell's symmetry axis and the laser propagation vector (\vec{Z} direction) to lift the degeneracy of ^{87}Rb hyperfine ground states into their respective Zeeman levels. The laser is a distributed-feedback laser diode emitting at 780 nm frequency stabilized on Rb D2 sub-Doppler absorption lines using a compact (1.4 cm^3) magnetically-shielded and thermally-controlled ^{87}Rb evacuated cell. An acousto-optical-modulator (AOM) is implemented in the LH and serves as a switch to control the duration and intensity of the laser pulses [45]. The AOM has the fall and rise times $< 5 \mu\text{s}$. The microwave synthesizer is used to generate the ≈ 6.835 GHz radiation for ^{87}Rb clock transition with a resolution below $1 \mu\text{Hz}$, and also controls the optical and microwave pulse sequences with a timing resolution at the level of $2 \mu\text{s}$, as used in the pulsed schemes [46]. All pulse durations and synchronization in the pulsed schemes are referenced to the high-stability quartz oscillator of the atomic clock setup, thus assuring a timing accuracy far below the nanosecond level over the duration of the pulse sequences employed (for typical pulse sequences, see sections 4.1, 4.3, and 4.4).

4. Characterization methods and results

We apply four methods, Franzen, CW-DR, Ramsey-DR and ODSE to measure the relaxation times in the buffer-gas ^{87}Rb vapor cell. The CW-DR and Ramsey-DR schemes were previously also used for analyses from a



metrological point of view including the short- and long-term frequency stability of our Rb atomic clock [47]. Franzen, Ramsey-DR and ODSE methods operate in pulse mode. In these three pulsed methods, first an optical pumping laser pulse creates a population imbalance by depopulating the ^{87}Rb $F_g = 2$ and filling the $F_g = 1$ ground state in the vapor cell (see figure 1). In the cases of Ramsey-DR and ODSE methods, optical pumping is followed by series of $\pi/2$ and/or π microwave pulses that create/modify coherence between the ground states. Finally—in all three pulse schemes—a laser probe pulse with the same frequency as during the optical pumping pulse is used to measure the optical density (OD) on the transition starting from $F_g = 2$ state by using a photodetector. To avoid re-pumping, this probe pulse has an approximately 100 times weaker intensity than the pump pulse. The variation of the OD as a function of time gives information about the population and/or coherence relaxation times. OD is defined to be the ratio of the incident I_0 and transmitted I_t laser probe pulse intensities:

$$\text{OD} = -\ln(I_t/I_0). \quad (7)$$

In the pulsed schemes, the laser probe pulse used for the detection does not resolve the atomic excited state because all the optical transitions to this $5^2\text{P}_{3/2}$ state are overlapped within Doppler linewidth. Furthermore, the clock transition cannot be addressed selectively by the laser alone either, because both the intrinsic transition linewidth and the Doppler linewidth are much larger than the Zeeman splitting in the $5\text{S}_{1/2}$ ground state. Hence, in these pulsed schemes, we can only address the population relaxation time between *all* m_F levels of the ground states $F_g = 1$ and $F_g = 2$ *simultaneously* (and not the clock transition only) which we write T_1' throughout this article. In Ramsey-DR and ODSE methods the frequency of the microwave field selects a particular hyperfine transition, which allows measuring its coherence relaxation time referring to the two involved m_F states only.

In the case of the CW-DR scheme, the linewidth of the resonance signal can be used to extract the coherence relaxation time for the clock transition. Also in the CW-DR scheme, the microwave frequency selects the specific Zeeman sublevels of interest. In all the above methods, no Doppler broadening occurs on the microwave transition, due to Dicke narrowing [43].

4.1. Franzen scheme

Franzen's well-known scheme of relaxation in the dark [12] for measuring population relaxation time is an all optical method, with absence of any microwave pulse. The timing sequence of the Franzen scheme is shown in inset in figure 3. First, a population imbalance is created between the ground states of ^{87}Rb atoms with the optical pumping. Then during the dark time T_{Dark} , the laser beam is switched off and the hyperfine population imbalance relaxes towards the thermal equilibrium. Finally, with a second laser pulse the sample's OD is probed which is a measure of the atomic population in $F_g = 2$. Figure 3 shows the experimentally obtained OD when T_{Dark} is varied, with the pump and probe pulse duration of 1 ms and 0.1 ms, respectively. By increasing the dark time, more atoms decay from $F_g = 1$ to $F_g = 2$ which results in increasing the OD. The data for the measurement is fitted with the equation:

$$\text{OD} = A - B \exp(-T_{\text{Dark}}/T_1'^{\text{Franzen}}), \quad (8)$$

where A , B and $T_1'^{\text{Franzen}}$ are the fitting parameters. As mentioned above, with this scheme only the population relaxation time of all m_F levels simultaneously is measured, which is determined as $T_1'^{\text{Franzen}} = 3.23$ (6) ms from

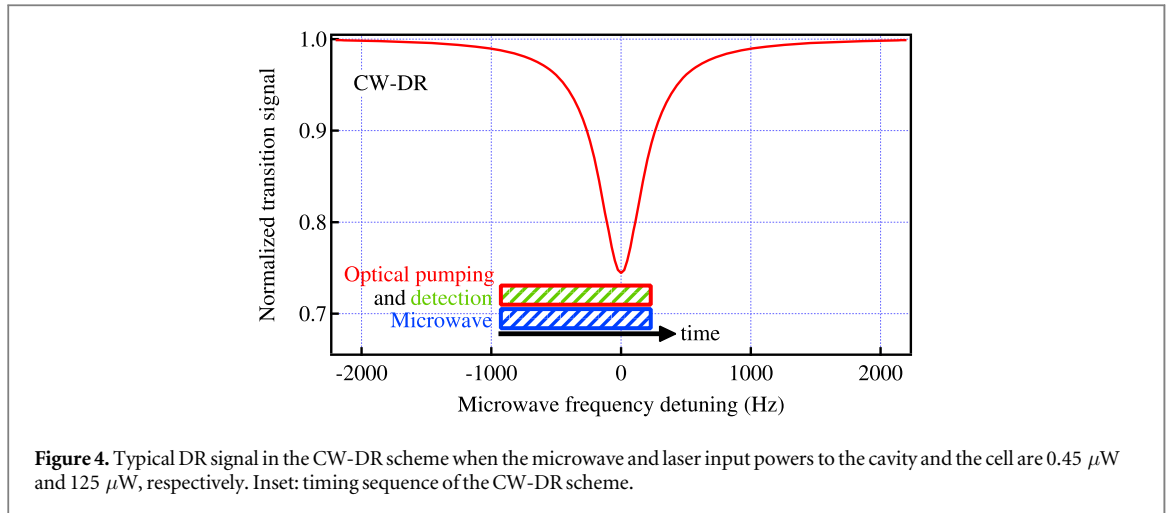


Figure 4. Typical DR signal in the CW-DR scheme when the microwave and laser input powers to the cavity and the cell are $0.45 \mu\text{W}$ and $125 \mu\text{W}$, respectively. Inset: timing sequence of the CW-DR scheme.

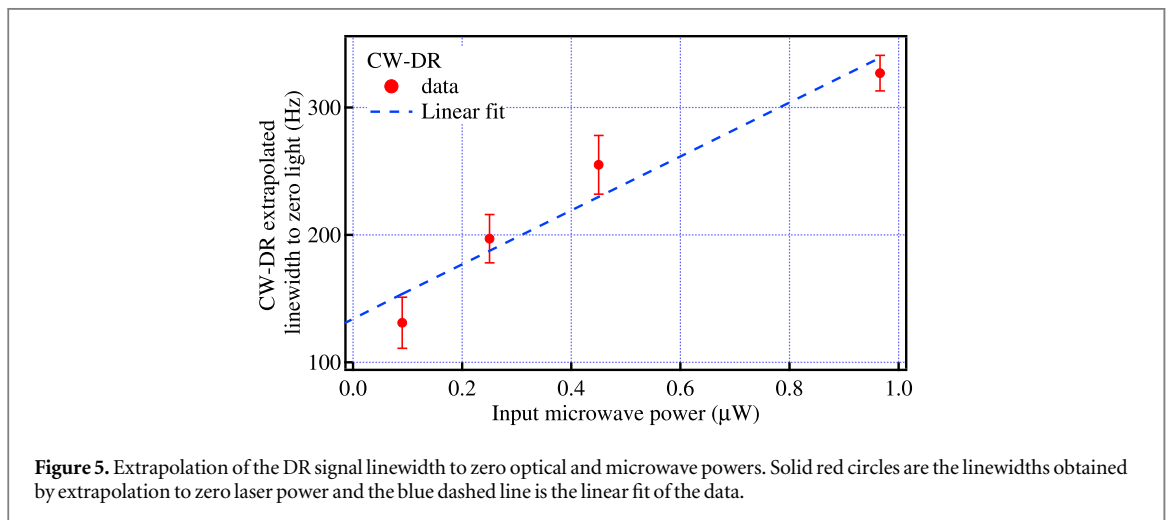


Figure 5. Extrapolation of the DR signal linewidth to zero optical and microwave powers. Solid red circles are the linewidths obtained by extrapolation to zero laser power and the blue dashed line is the linear fit of the data.

equation (8). This result did not change significantly when the measurement was repeated with the pump and probe pulse durations varied by $\pm 50\%$.

4.2. CW-DR scheme

In the case of CW-DR scheme [30], the laser optically pumps the Rb atoms in the vapor, while simultaneously a microwave field near-resonant with the ^{87}Rb hyperfine clock transition is applied. The transmitted light signal as a function of microwave frequency is a measure of the atomic ground state polarization known as DR signal. Figure 4 shows a typical DR signal which is obtained when the microwave frequency is scanned near resonance with $0.45 \mu\text{W}$ input power to the cavity and with $125 \mu\text{W}$ optical power to the cell. The linewidth of the DR signal is a measure of the coherence relaxation rate [32], but is additionally increased by optical and microwave power broadenings. To correct for this power broadening, the intrinsic DR signal linewidth, $\Delta\nu_{1/2}$, is determined by extrapolating the measured linewidth to zero with respect to both the optical and microwave powers, figure 5. By using this method, a coherence relaxation time for the clock transition, which is selectively driven by the applied microwave, is found to be $T_2^{*\text{CW-DR}} = (\pi\Delta\nu_{1/2})^{-1} = 2.4(4) \text{ ms}$ [3]. However, this $T_2^{*\text{CW-DR}}$ is significantly smaller than the predicted intrinsic T_2 from table 1. This can be attributed to uncertainties in the extrapolations and to additional relaxation due to gradients of the static magnetic field in the vapor cell which are well-known from NMR [40, 41].

4.3. Ramsey-DR scheme

In the Ramsey-DR scheme [48, 49], the three steps of optical pumping, microwave interrogation and optical detection are separated in time, see inset in figure 6. First, during the optical pumping a strong laser pulse creates a population imbalance between the two ground-state sublevels of ^{87}Rb . The optical pumping pulse has an input power to the vapor cell on the level of 14 mW and a duration of 0.4 ms . After this pumping pulse, in absence of light, two coherent $\pi/2$ microwave pulses are applied that are separated by the Ramsey time T_R . Both microwave

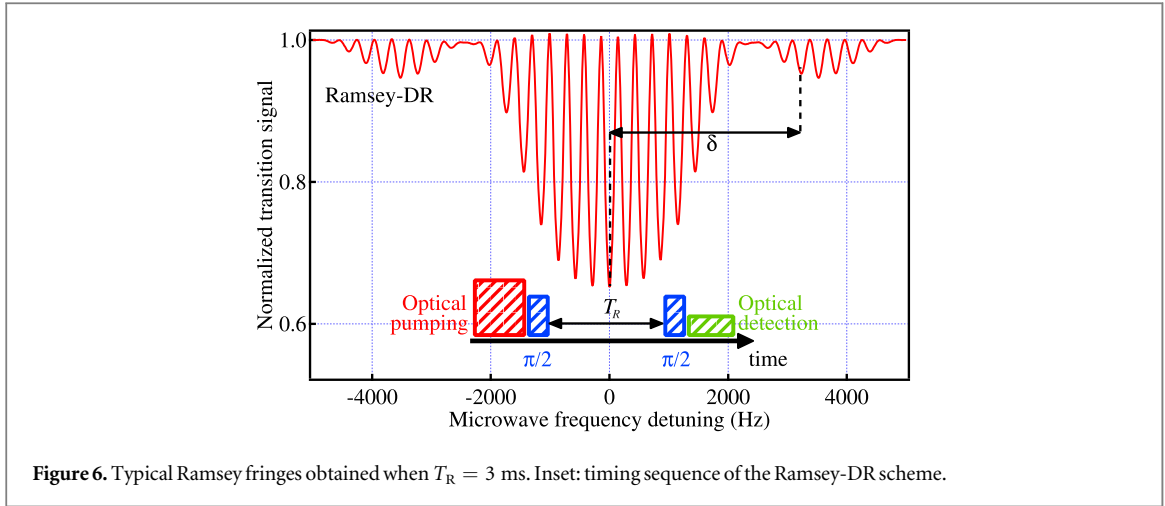


Figure 6. Typical Ramsey fringes obtained when $T_R = 3$ ms. Inset: timing sequence of the Ramsey-DR scheme.

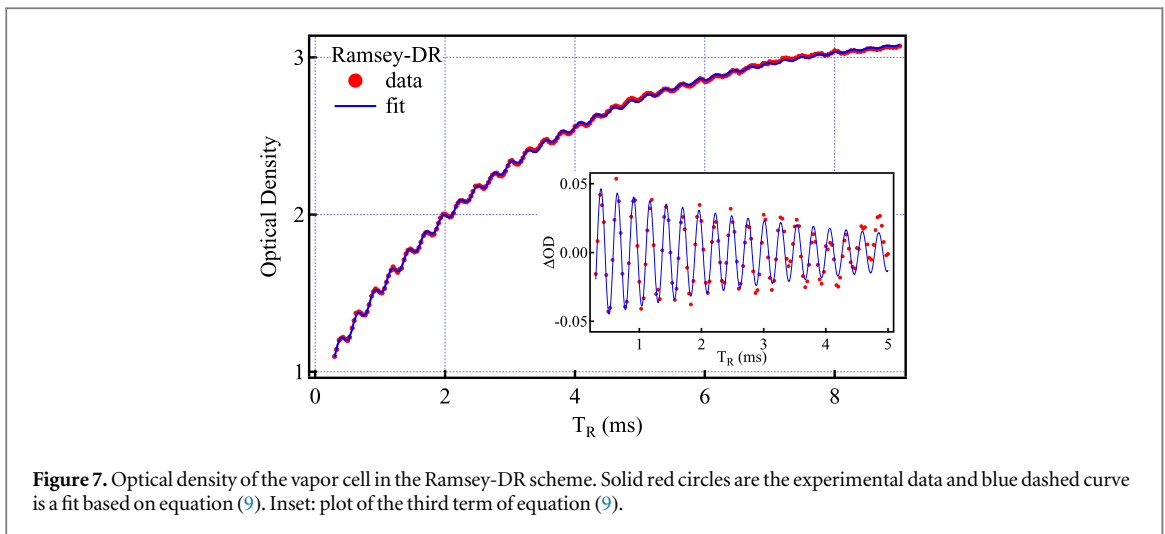


Figure 7. Optical density of the vapor cell in the Ramsey-DR scheme. Solid red circles are the experimental data and blue dashed curve is a fit based on equation (9). Inset: plot of the third term of equation (9).

pulses have the same duration of 0.4 ms, the same amplitude corresponding to a power of -18.2 dBm injected to the cavity and the same microwave frequency. The amplitude and duration of the $\pi/2$ microwave pulses in our Rb atomic clock were optimized according to the Rabi oscillation method presented in [50].

On the atomic level, the first $\pi/2$ microwave pulse creates a coherent superposition of the two hyperfine $m_F = 0$ states involved in the clock transition. During the Ramsey time, atoms evolve freely at the Larmor frequency. The second resonant microwave pulse converts the accumulated atomic phase into a population difference between the hyperfine states. Finally, in the last sequence the optical detection takes place with the laser. The laser frequency is the same for both optical pumping and detection steps, but the laser intensity is about 100 times weaker during the detection. In the Ramsey-DR scheme, the optical detection pulse duration is 0.7 ms [51] which results in an overall duration of one complete interrogation cycle of the scheme equal to $T_R + 1.9$ ms.

Figure 6 shows typical detected Ramsey fringes obtained by varying the microwave pulse frequency around the clock transition frequency, here for a Ramsey time of $T_R = 3$ ms. The OD of the Rb vapor is recorded for various values of T_R , with the microwave detuned from the clock transition by a fixed detuning δ (see figure 6) [16]. Figure 7 shows the recorded OD as a function of Ramsey time when the cavity is placed in a static magnetic field of 40 mG and the frequency of the microwave field is detuned from the resonance by $\delta = 3.8$ kHz. The data is fitted with the function [16]:

$$OD = A - B \exp(-T_R/T_1^{\text{Ramsey}}) + C \exp(-T_R/T_2^{\text{Ramsey}}) \sin(2\pi\delta T_R + \varphi), \quad (9)$$

where $A, B, C, T_1^{\text{Ramsey}}, T_2^{\text{Ramsey}}, \delta$ and φ are the fitting parameters. The fit gives the relaxation times with uncertainties $T_1^{\text{Ramsey}} = 3.20(1)$ ms and $T_2^{\text{Ramsey}} = 3.95(25)$ ms. Inset of figure 7 is the plot of the third term of equation (9) which shows the Ramsey oscillations in better contrast than the OD plot in figure 7.

In this method, like in the Franzen method, the T_1^{Ramsey} is a measurement of the population relaxation time for all m_F levels confounded and it is consistent with T_1^{Franzen} . However in contrast to the T_1^{Ramsey} population

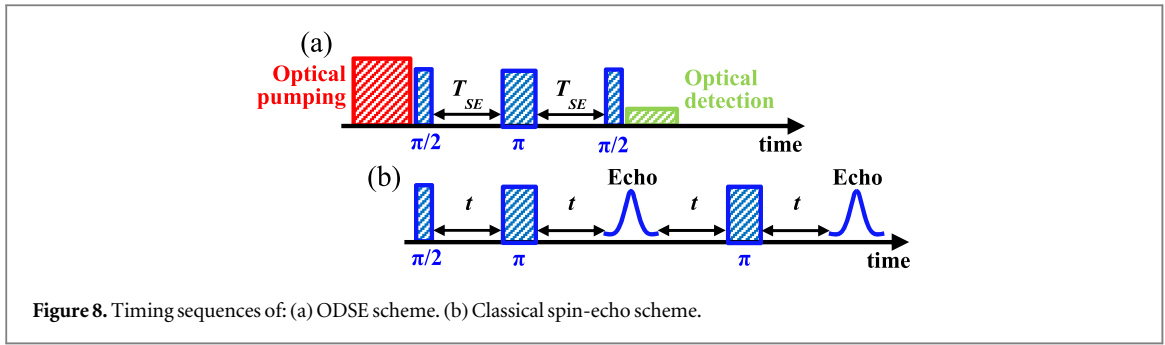


Figure 8. Timing sequences of: (a) ODSE scheme. (b) Classical spin-echo scheme.

relaxation time, $T_2^{*\text{Ramsey}}$ refers to the coherence relaxation time specific for the clock transition alone [16]. It is longer than T_2 from CW-DR method, but this $T_2^{*\text{Ramsey}}$ is still significantly shorter than the predicted coherence relaxation time ($T_2 = 4.5$ ms) from section 2. A likely reason for this can be the presence of the inhomogeneity of the static magnetic field inside our vapor cell that motivated us to propose our ODSE method to suppress this effect and measure the intrinsic T_2 (see section 4.4). Although, we note that such static magnetic field gradients are generally small across the vapor cell in our atomic clock, for example on the order of 4% in a similar physics package (see [52]).

In addition to the relaxation times, the microwave detuning from the resonance—which is given by the Ramsey oscillations—is obtained from the fit to equation (9) to be $\delta = 3.8 \pm 0.003$ kHz which is in excellent agreement with the measurement conditions.

4.4. ODSE scheme

In order to suppress coherence relaxation due to static magnetic field gradients (see section 2), we propose the new scheme of ODSE. The ODSE method is inspired by the NMR spin-echo method presented by Hahn [21] which is used to narrow the resonance line broadening in inhomogeneous static magnetic fields.

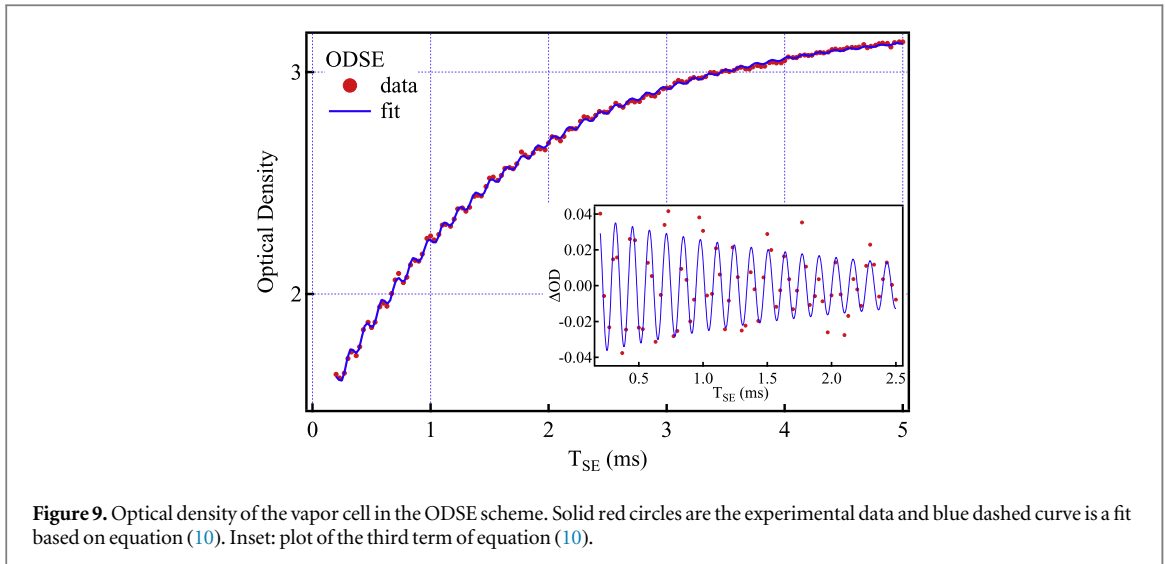
In classical NMR spin-echo, a pickup coil is required to detect the magnetic moments' precession of the sample [40], which on one hand cannot easily be integrated into an atomic clock using a microwave cavity and on the other hand can collect noise from the cell and reemit the collected microwaves through the wires outside of the cell, thus producing additional noise. In the proposed ODSE method a photodetector is used to measure the OD in the vapor cell which is much more robust, reliable and does not feedback noise to the atoms, thus circumventing the problems existing in the standard method of detection using pickup coil.

In the Ramsey-DR scheme, after the first $\pi/2$ microwave pulse, because of the inhomogeneity of the static magnetic field, the atomic spins dephase at different rates and their coherence starts to decay which finally results in a shorter coherence relaxation time compared to the intrinsic T_2 . To suppress this effect—like in NMR spin-echo—we apply a π microwave pulse added between the $\pi/2$ microwave pulses of the Ramsey-DR method and propose this resulting ODSE method for relaxation time measurements in an atomic vapor cell (see figure 8(a)). In the ODSE method, all the experimental conditions of optical pumping, optical detection and $\pi/2$ microwave pulses are the same as for the Ramsey-DR scheme (see section 4.3). The additional π pulse is separated from each of the two $\pi/2$ pulses by a dephasing time T_{SE} and has the same frequency and amplitude as the $\pi/2$ pulses, but its duration is two times longer so the duration of one complete cycle of ODSE scheme becomes $2T_{SE} + 2.7$ ms. The π pulse flips the direction of dephasing spins and reverses the spin phases (spin-flips). After some time equal to the dephasing time, T_{SE} , the dephased states are rephased at the instant of the second $\pi/2$ microwave pulse. Finally, the detection by the second $\pi/2$ pulse and the laser pulse destroys the atomic coherences so no more consecutive echoes (as observed in NMR, see figure 8(b)) can be detected. The OD of the vapor sample is recorded by varying the rephasing (and dephasing) time T_{SE} , with the same experimental conditions as in the case of Ramsey-DR scheme, i.e. a static magnetic field of 40 mG and microwave frequency detuning of $\delta = 3.8$ kHz from the clock transition. Like in the Ramsey-DR method, a trade-off exists for selecting δ in the ODSE method: for very small δ , big initial variations in I_t and thus in OD can be observed, but only few oscillations occur before they are damped away after about T_R or $T_{SE} \approx 2 \cdot T_2$. For very big δ on the other hand, many oscillations can be observed over this timescale but the maximum variation of I_t is small, which reduces the signal-to-noise ratio of the OD data.

The experimental data shown in figure 9 is fitted to the function:

$$\text{OD} = A - B \exp(-2T_{SE}/T_1^{\text{ODSE}}) + C \exp(-2T_{SE}/T_2^{\text{ODSE}}) \sin(4\pi\delta T_{SE} + \varphi), \quad (10)$$

where $A, B, C, T_1^{\text{ODSE}}, T_2^{\text{ODSE}}, \delta$ and φ are the fitting parameters. The fit gives both the relaxation times of $T_1^{\text{ODSE}} = 3.21$ (5) ms and $T_2^{\text{ODSE}} = 4.30$ (85) ms and $\delta = 3.8 \pm 0.005$ kHz. T_1^{ODSE} refers to the population relaxation time for the transitions between all m_F levels (like in the Franzen and Ramsey-DR methods). It shows



a very good consistency with the obtained T_1' from Franzen and Ramsey-DR methods. The measured T_2^{ODSE} is in a good agreement with the predicted intrinsic coherence relaxation time T_2 (≈ 4.5 ms).

In our proof-of-principle experiment, the measured relaxation times in ODSE method have larger uncertainties (3–5 times) compared to the ones from the Ramsey-DR method. We attribute this phenomena to: (1) the ODSE signal has a lower amplitude than the Ramsey-DR signal which is due to the longer duration of one complete interrogation cycle (2.7 ms + $2T_{\text{SE}}$ versus 1.9 ms + T_{R}), and (2) the residual instabilities of the microwave-synthesizer frequency over the entire measurement duration of about two hours may introduce additional noise on the signal (in Ramsey-DR and ODSE methods about 250 (figure 7) and 150 (figure 9) data points are presented, respectively).

To demonstrate the enhanced immunity of the ODSE method to inhomogeneity in the static magnetic field, the measurements were repeated with both Ramsey-DR and ODSE methods when the static magnetic field was doubled to 80 mG—resulting also in doubling of the static magnetic field gradient dominated by the geometry of the field coil—while all other parameters were kept unchanged. Under these conditions, with ODSE scheme the coherence relaxation time was measured to be $T_2^{\text{ODSE}} = 4.26$ (80) ms which is consistent to better than 1% with the measured coherence relaxation time when the magnetic field was 40 mG. But in the case of the Ramsey-DR scheme at higher magnetic field, the coherence relaxation time was measured to be $T_2^{\text{Ramsey}} = 3.80$ (25) ms which is about 4% shorter compare to $T_2^{\text{Ramsey}} = 3.95$ (25) ms obtained with lower magnetic field and its gradient. This comparison shows that the ODSE scheme is a promising method to suppress the effect of inhomogeneity of the static magnetic field across the vapor cell, even in the case of our well-controlled clock physics package with its highly homogeneous magnetic field.

5. Conclusion

We have introduced and demonstrated the method of ODSE to determine the population relaxation time (for all m_F -levels of the $F_g = 1$ and $F_g = 2$ ground states simultaneously) and the intrinsic coherence relaxation time, T_2 , specifically for the clock transition in a thermal atomic vapor with buffer-gas in view of its application to atomic clocks. This method was compared to other well established Franzen, CW-DR and Ramsey-DR methods using the same ^{87}Rb vapor cell. The population relaxation time measured with the ODSE method was very consistent with the ones from Franzen and Ramsey-DR methods. In all those pulsed methods, the obtained population relaxation time measured for all m_F -levels simultaneously (and not only for the clock transition). We have shown that the ODSE method suppresses coherence relaxation arising from gradients in the static magnetic field across the vapor cell and thus yields the intrinsic coherence relaxation time closer to the theoretically predicted T_2 . In contrast, the measured coherence relaxation times by both CW-DR and Ramsey-DR methods were shorter than the predicted T_2 , due to the inhomogeneity of the magnetic field.

Our proof-of-principle demonstrations shows that ODSE is a highly useful tool for measuring intrinsic relaxation rates in atomic vapors, independently of present magnetic field gradients. By measuring T_2 times with both the ODSE and Ramsey-DR schemes, it should also be possible to obtain experimental information on the magnetic field gradients across the atomic sample or vapor cell under study. Contrary to NMR spin-echo, our ODSE method does not need any pickup-coil but uses a photodetector to record the light absorbed in the vapor cell (OD), which is more robust and less noisy than detection in the radio-frequency or microwave regime.

Moreover, the photodetector can be conveniently placed outside the atomic vapor system under study—in our case outside the entire vapor-cell clock physics package—which makes the ODSE method an ideal candidate for characterizing relaxation times in atomic clocks with a cavity. While not covered by this present study, it would be of interest to study a potential extension of the ODSE technique to less localized atomic systems such as vapor cells without buffer-gas but equipped with an anti-relaxation wall coating. Similarly, the ODSE method is of high interest for characterizing relaxation rates in other quantum optics systems with optical readout, such as quantum information storage or processing [5, 53], cold-atom experiments [54], and other applications of quantum systems that rely on long-live atomic coherences.

Acknowledgments

This work was supported by the Swiss National Science Foundation (SNSF grants no. 140712 and 162346), the European Metrology Research Programme (EMRP project IND55-Mclocks), SNSF-Scopes project (152511) and Ministry of Education, Science and Technological Development of Republic Serbia (III 45016 and OI 171038) and COST Action 1403 Nanoscale Quantum Optics. The EMRP is jointly funded by the EMRP participating countries within EURAMET and the European Union. We thank A K Skrivervik and A Ivanov (both EPFL-LEMA) for their support on the microwave cavity, C Calosso (INRIM, Italy) for providing the microwave LO, W Moreno and M Pellaton (both LTF) for helpful discussions. We thank our former colleague S Kang for his contributions to the early phases of the work.

References

- [1] Keeler J 2010 *Understanding NMR Spectroscopy* 2nd edn (Chichester: Wiley)
- [2] Budker D and Romalis M 2007 *Nat. Phys.* **3** 227
- [3] Vanier J and Audoin C 1989 *The Quantum Physics of Atomic Frequency Standards* (Bristol: Adam Hilger)
- [4] Camparo J 2007 *Phys. Today* **60** 33
- [5] Julsgaard B, Kozhekin A and Polzik E S 2001 *Nature* **413** 400
- [6] Knappe S 2007 Emerging topics: MEMS atomic clocks *Comprehensive Microsystems* ed Y Gianchandani et al vol 3 (Amsterdam: Elsevier) p 571–612
- [7] Dupuis RT, Lynch T J and Vaccaro J R 2008 *Proc. IEEE Int. Frequency Control Symp.* ed B Jadsliwer (*Honolulu, Hawaii, USA, 19–21 May 2008*) pp 655–60
- [8] Waller P, Gonzalez S, Binda S, Sesia I, Hidalgo I, Tobias G and Tavella P 2010 *IEEE Trans. Ultrason. Ferroelect. Freq. Control* **57** 738
- [9] Chunhao H, Zhiwu C, Yuting L, Li L, Shenghong X, Lingfeng Z and Xianglei W 2013 *Int. J. Navig. Obs.* **2013** 371450
- [10] Kuzmich A, Mandel L and Bigelow N P 2000 *Phys. Rev. Lett.* **85** 1594
- [11] Budker D, Gawlik W, Kimball D F, Rochester S M, Yashchuk V V and Weis A 2002 *Rev. Mod. Phys.* **74** 1153
- [12] Franzen W 1959 *Phys. Rev.* **115** 850
- [13] Liberman V and Knize R J 1986 *Phys. Rev.* **34** 5115
- [14] Graf M T, Kimball D F, Rochester S M, Kerner K, Wong C and Budker D 2005 *Phys. Rev. A* **72** 23401
- [15] Corsini E P, Karaulanov T, Balabas M and Budker D 2013 *Phys. Rev. A* **87** 22901
- [16] Horsley A, Du G X, Pellaton M, Affolderbach C, Mileti G and Treutlein P 2013 *Phys. Rev. A* **88** 063407
- [17] Budker D, Hollberg L, Kimball D F, Kitching J, Pustelny S and Yashchuk V V 2005 *Phys. Rev. A* **71** 012903
- [18] Castagna N and Weis A 2011 *Phys. Rev. A* **84** 053421
Castagna N and Weis A 2012 *Phys. Rev. A* **85** 059907 (erratum)
- [19] Scholtes T, Woetzel S, IJsselstein R, Schultze V and Meyer H G 2014 *Appl. Phys. B* **117** 211
- [20] Castagna N, Bison G, Di Domenico G, Hofer A, Knowles P, Macchione C, Saudan H and Weis A 2009 *Appl. Phys. B* **96** 763
- [21] Hahn E L 1950 *Phys. Rev.* **80** 580
- [22] Bar-Gill N, Pham L M, Jarmola A, Budker D and Walsworth R L 2013 *Nat. Commun.* **4** 1743
- [23] Hodges J S, Yao N Y, Maclaurin D, Rastogi C, Lukin M D and Englund D 2013 *Phys. Rev. A* **87** 032118
- [24] Viola L and Lloyd S 1998 *Phys. Rev. A* **58** 4
- [25] Shim J H, Niemeyer I, Zhang J and Suter D 2012 *Europhys. Lett.* **99** 4
- [26] Hosseini M, Sparkes B M, Campbell G, Lam P K and Buchler B C 2011 *Nat. Commun.* **2** 174
- [27] Tittel W, Afzelius M, Chaneilière T, Cone R L, Kröll S, Moiseev S A and Sellars M 2010 *Laser Photon. Rev.* **4** 244–67
- [28] Laplane C, Jobez P, Etesse J, Timoney N, Gisin N and Afzelius M 2016 *New J. Phys.* **18** 013006
- [29] Wolfowicz G, Maier-Flaig H, Marino R, Ferrier A, Vezin H, Morton J J L and Goldner P 2015 *Phys. Rev. Lett.* **114** 170503
- [30] Bandi T, Affolderbach C, Stefanucci C, Merli F, Skrivervik A K and Mileti G 2014 *IEEE Trans. Ultrason. Ferroelect. Freq. Control* **61** 1769–78
- [31] Kang S, Gharavipour M, Gruet F, Affolderbach C and Mileti G 2015 *Proc. Joint Conf. IEEE Int. Frequency Control Symp. & European Frequency and Time Forum (EFTF) (Denver, Colorado, USA, 12–16 April 2015)* pp 800–3
- [32] Vanier J and Mandache C 2007 *Appl. Phys. B* **87** 565–93
- [33] Oretto P J, Jau Y Y, Post A B, Kuzma N N and Happer W 2004 *Phys. Rev. A* **69** 042716
- [34] Robinson H G, Ensberg E S and Dehmelt H G 1958 *Bull. Am. Phys. Soc.* **3** 9
- [35] Bouchiat M A and Brossel J 1966 *Phys. Rev.* **147** 41
- [36] Bandi T, Affolderbach C and Mileti G 2012 *J. Appl. Phys.* **111** 124906
- [37] Vanier J, Simard J F and Boulanger J S 1974 *Phys. Rev. A* **9** 1031
- [38] Franz F A and Lüsher E 1964 *Phys. Rev.* **135** A582
- [39] Franz F A 1965 *Phys. Rev.* **139** A603
- [40] Carr H Y and Purcell E M 1954 *Phys. Rev.* **94** 630–8

- [41] Torrey H C 1956 *Phys. Rev.* **104** 563–5
- [42] Risley A, Jarvis S Jr and Vanier J 1980 *J. Appl. Phys.* **51** 4571
- [43] Dicke R H 1953 *Phys. Rev.* **89** 472
- [44] Stefanucci C, Bandi T, Merli F, Pellaton M, Affolderbach C, Mileti G and Skrivervik A K 2012 *Rev. Sci. Instrum.* **83** 104706
- [45] Gruet F, Pellaton M, Affolderbach C, Bandi T, Matthey R and Mileti G 2012 *Proc. Int. Conf. on Space Optics (ICSO) (Ajaccio, Corsica, 9–12 October 2012)* no 48
- [46] Calosso C E, Micalizio S, Godone A, Bertacco E K and Levi F 2007 *IEEE Trans. Ultrason. Ferroelectr. Freq. Control* **54** 1731
- [47] Gharavipour M, Affolderbach C, Kang S, Bandi T, Gruet F, Pellaton M and Mileti G 2016 *J. Phys.: Conf. Ser.* **723** 012006
- [48] Ramsey N 1956 *Molecular Beams* (Oxford: Oxford University Press)
- [49] Micalizio S, Godone A, Levi F and Calosso C 2009 *Phys. Rev. A* **79** 013403
- [50] Kang S, Gharavipour M, Affolderbach C, Gruet F and Mileti G 2015 *J. Appl. Phys.* **117** 104510
- [51] Kang S, Gharavipour M, Affolderbach C and Mileti G 2015 *Electron. Lett.* **51** 1767–9
- [52] Affolderbach C, Du G, Bandi T, Horsley A, Treutlein P and Mileti G 2015 *IEEE Trans. Instrum. Meas.* **64** 3629–37
- [53] Ardavan A, Rival O, Morton J J L, Blundell S J, Tyryshkin A M, Timco G A and Winpenny R E P 2007 *Phys. Rev. Lett.* **98** 057201
- [54] Maineult W, Deutsch C, Gibble K, Reichel J and Rosenbusch P 2001 *Phys. Rev. Lett.* **109** 020407

Slow and Stored Light in Amplifying Four Way Mixing Process

Bojan Zlatković, Aleksandar Krmpot, Ivan Radojičić, Dušan Arsenović, Milan Minić,
and Brana Jelenković

Institute of physics, University of Belgrade, Pregrevica 118, 11080 Belgrade, Serbia

Tel: (38111) 3713 107, e-mail: branaj@ipb.ac.rs

ABSTRACT

We have investigated experimentally and theoretically four-wave mixing (FWM) in hot potassium vapor as a medium for producing slow and store light. Two pump and a single probe photon were mixed in double- Λ system, characterized by parametric amplification of coupled co-propagating probe and conjugate beams. We have observed very high gains of probe and conjugate, up to 60 and 80 respectively, at two photon Raman resonance, under large one photon detuning, and high K-cell temperature. Using an amplifying medium to alleviate the absorption and distortion of propagating pulses are important for slow-light propagation. We observed ultraslow propagation of probe and conjugate pulses under conditions when parametric amplification of twin beams is well below their maximum values. A fractional delays of close to 5 at a gain ~ 1.5 , for the probe pulse of 20 ns, have been achieved simultaneously for both probe and accompanying conjugate pulse. FWM mixing process under conditions of the experiment results in broadening of twin beams, close to observed delays.

Keywords: four way mixing, electromagnetically induced transparency, slow light, potassium.

1. INTRODUCTION

Four-wave mixing (FWM) in the double lambda configuration in alkalis has been intensively studied since electromagnetically induced transparency (EIT) in double-atomic systems allows control of the FWM process, and often brings large parametric gains of twin beams, probe and conjugate. There are only few works on FWM in potassium vapor [1,2], all done with counter propagating pump and probe beams. On the other hand, potassium ^{39}K ground state hyperfine splitting is only 461 MHz, lower than in any other alkali atom, In potassium, transitions originating from both ground state hyperfine sublevels are completely overlapped because of Doppler broadening. This affects the dynamics of pumping and repopulating ground state hyperfine sublevels in a different way than in other alkali atoms. Moreover, atomic susceptibilities that govern the FWM process should be higher in atoms with lower hyperfine splitting [3].

In this work we have studied slow light in hot K vapor under different parametric gains of twin beams. The transmission line shape of the twin beams under FWM conditions look like a Lorentzian transmission, and the dispersion within the gain profile give rise to slow light. We have investigated, experimentally and theoretically, gains of twin beams and their fractional delays and broadening under different two photon Raman detuning, one photon (pump) detuning, K atom density and pump beam intensity.

In the experiment and in the model, pump and probe beams are co-propagating and intersect under a small angle in the K - cell. Probe and conjugate are detected as they exit the cell. This scheme is suitable to investigate other properties of FWM, like relative intensity squeezing between twin beams, since FWM has been identified as a very efficient process to generate non classical beams [4].

We show experimentally and numerically that a double-Lambda system in K vapor, characterized by parametric amplification of coupled probe and four-wave mixing pulses, is promising medium for producing slow light and also stored light. Moreover, this system can compensate for the absorption and broadening processes that usually occur without destroying the coherent properties of the medium. We are currently experimenting with storage of light pulses in Potassium.

2. EXPERIMENT AND MODEL

We use co-propagating orthogonally polarized pump and probe to couple three hyperfine levels via double- Λ scheme in D1 line in ^{39}K (Fig. 1a).

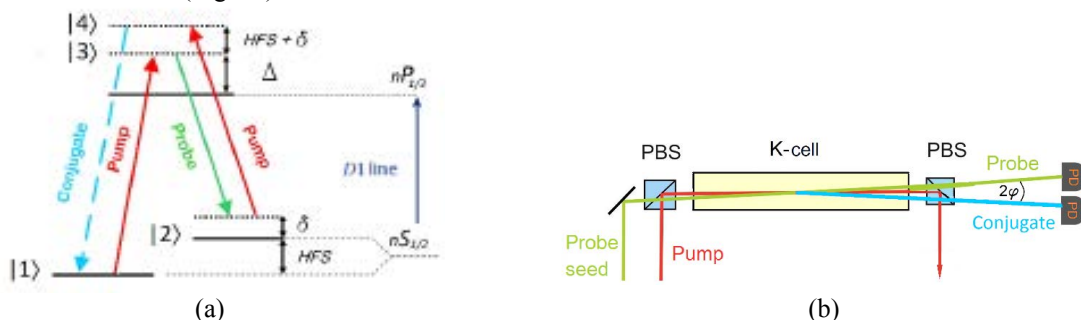


Figure 1. Schematic of a) atomic level diagram for FWM in K and b) experimental the setup.

Level $|3\rangle$ from Fig. 1 is $4P_{1/2}$ while two lower levels $|1\rangle$ and $|2\rangle$ are $4S_{1/2}$, $F=1$ and $4S_{1/2}$, $F=2$ respectively. Important feature of this set up (Fig. 1b) is the amplification in the FWM process and generation of the conjugate pulse, coupled to the probe and propagating alongside the probe.

In the experiment (Fig. 1b) pump (red) and probe (green) are combined on the polarization beam splitter (PBS). They intersect at a small angle φ inside the potassium vapor cell (K-cell). Exciting the cell are probe and conjugate (blue), detected by two photodiodes. The only light source is the single mode, frequently stabilized Ti:Sapphire at ~ 770 nm, used for both pump and probe seed beams. The probe seed (≈ 200 μ W), derived by extracting a small fraction of the pump is frequency shifted by the pair of AOM making the overall frequency offset between pump and probe close to the hyperfine splitting of the ^{39}K ground state. Two-photon detuning δ is scanned by changing the RF frequency fed to one of the AOM. The K cell temperature and thus the density of K atoms are controlled by the temperature of hot air flowing inside the ceramic cylinder with the K cell.

To obtain the physical insight in to the FWM processes, we first solve the Maxwell-Bloch equations for the probe and FWM fields and then the coupled equations for field propagation, equations (1) and 2),

$$\frac{d\hat{\rho}}{dt} = -\frac{i}{\hbar} [\hat{H}_A + \hat{H}_{AF}, \hat{\rho}] + S\hat{E} + \gamma(\hat{\rho}_0 - \hat{\rho}) \quad (1)$$

$$\left(\frac{\partial}{\partial z} + \frac{1}{c} \frac{\partial}{\partial t} \right) E^{(+)} = i \frac{k}{2\epsilon_0} P^{(+)} \quad (2)$$

where \hat{H}_A and \hat{H}_{AF} are free and atom-laser interaction Hamiltonians, $S\hat{E}$ denotes spontaneous emission, γ is relaxation rate to ground states $\hat{\rho}_0$, $E^{(+)}$ is positive frequency part of the electric fields and $P^{(+)}$ for macroscopic polarizations.

3. RESULTS AND DISCUSSION

We first made detailed analyses of parameters that affects gains of the probe and conjugate. Next, we compared waveforms of the reference (probe pulse before the K – cell) with the probe and conjugate pulses behind the cell for conditions corresponding to different gain levels. Optimal parameters for probe and conjugate gains, and for time delays between reference probe and probe and conjugate exciting the K-cell were selected after varying pump intensity, K-cell temperature (gas density), OPD and TPD.

3.1 Gain of Probe and Conjugate

We have investigated the dependence of the probe and the conjugate gain on two-photon detuning δ (TPD), one-photon detuning Δ (OPD), pump laser intensity and the density of K atoms. The gain of the probe and the conjugate is defined as $G_p = P_p/P_{p,in}$ and $G_c = P_c/P_{c,in}$, where P_p and P_c are measured powers of the probe and the conjugate, respectively, and P_{in} is initial power of the probe seed inside the amplifying medium.

Optimal parameters for high probe and conjugate gains are summarized in Fig. 2 where we have shown gains as a function of TPD for various OPD, for K cell temperature of 120 $^{\circ}\text{C}$ ($\approx 3 \times 10^{12}$ atoms/cm 3), pump power of 400 mW and the probe seed power of 200 μ W. The angle between the pump and the probe was $\varphi = 3$ mrad.

The maximal gains of the probe and the conjugate were ~ 80 and ~ 60 respectively, for OPD = 700 MHz and TPD = -6 MHz. The maximum of gains at a particular OPD is due to competition between photon amplification and absorption^{13,20}. The trade-off is for OPD ~ 700 MHz which is close to Doppler broadening in K. Since the frequency of the conjugate is offset much further from the hyperfine splitting, for $\sim 2 \times 460$ MHz = 920 MHz, its absorption is weaker than the probe., leading to higher gains for the conjugate, as long as OPD is not very large, for instance over 1.3 GHz.

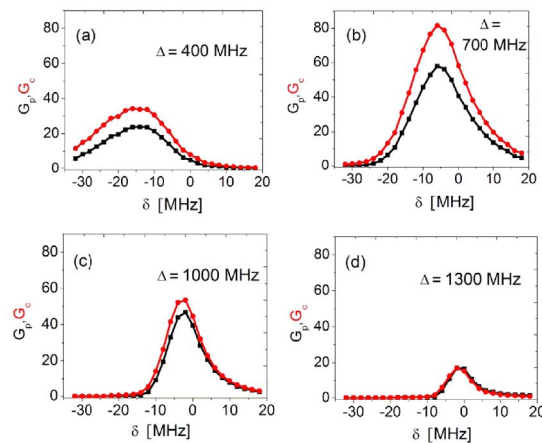


Figure 2. Schematic of a) atomic level diagram for FWM in K and b) experimental setup.

3.2 Slow Light

The probe pulses were either Gaussian or triangle. The necessary fast (10 – 100 ns) quasi-Gaussian excitation pulse was made by the fine shaping of the trapezoid pulse with a passive CLC pi-filter. Parameters of the trapezoid pulse (height, FWHM and rise time) were obtained by fitting the unit-height and unit-half-width Gaussian pulse with the symmetrical trapezoid waveform, in the range of ± 5 . After appropriate scaling for the half-widths of necessary Gaussian pulses, these optimal trapezoidal pulses were made by a pulse generator and sent to the CLC pi-filter with 50 ohms characteristic impedance and characteristic time constant $2\pi\sqrt{LC}/2$ equal to the pulse FWHM. In this way the breakpoints of the trapezoid pulse were well filtered with only a small asymmetry added. Each quasi-Gaussian pulse was generated with its own appropriate filter. The pulse was sent to EOM for shaping the fast probe pulse.

The main parameters affecting the propagation of twin beams, pulse fractional delays and broadening are pump power and pump OPD. Waveforms of the input (reference) probe and the probe and conjugate pulse at the output of the cell, for 20 ns reference pulse, OPD = 1.5 GHz, TPD = -1 MHz at the temperature of the cell 130 °C are given in Fig. 3.

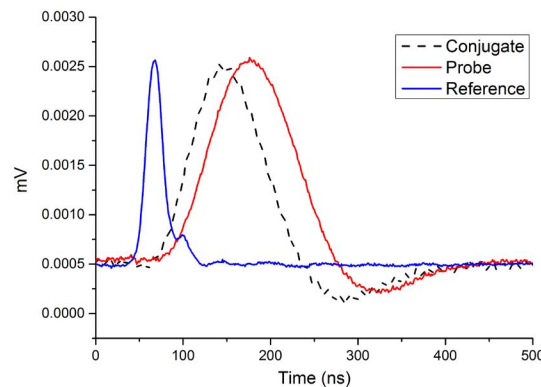


Figure 3. Waveforms of the reference (solid blue), probe (solid red) and conjugate (dashed black) at low gain and high OPD. The pump power was 400 mW, the probe power was OPD = 1.5 GHz.

The delay time of both probe and conjugate can be made longer when the gain is set lower. The conjugate pulse always precedes the probe pulse. Like in sodium [5] the model gives wider pulses at the output of the cell than what we observed. The theory and numerical simulation show similar behavior of twin beams. In the low pump power and low-gain regime the probe-pulse velocity is close to the EIT group velocity, at a low gain high pump power the conjugate velocity can be nearly twice as the probe. In the high-gain regime, the probe accelerates and twin beams propagate with the similar velocity $v_s = 2v_g$.

4. CONCLUSIONS

We explored experimentally and numerically generation process of non-degenerate FWM in Potassium, under double-Lambda atomic scheme. We have observed exceptionally high gain of twin beams, around 60 and 80 for probe and conjugate, under moderate pump power of 400 mW, near the Raman resonance of the pump and the probe, and at one-(pump) photon detuning close to Doppler broadening in K. Such high gain can be attributed to high atomic susceptibility in K, i.e., the lowest hyperfine splitting of the ground state of all alkalis.

We have shown slow light propagation of twin beams, with the conjugate pulse exciting the cell first. For very short input probe pulses of 10 – 20 ns, ultra-slow light effect and large fractional delay of 5 are observed. Pulse broadening at the cell output is large, nearly large as the delay between the reference pulse and the probe. Further optimization of parameters should help in narrowing the pulse widths, which is very important for applications of such systems in pulse repetition mode.

ACKNOWLEDGEMENTS

Authors acknowledge grant III45016 of the Serbian Ministry of education and science and technological development.

REFERENCES

- [1] D. S. Glassner and R. J. Knize: Reduced angular dependence for degenerate four-wave mixing in potassium vapor by including nitrogen buffer gas, *Appl. Phys. Lett.*, vol. 66, pp. 1593-1595 (1995).
- [2] M. Y. Lanzerotti *et al.*: High-reflectivity, wide-bandwidth optical phase conjugation via four-wave mixing in potassium vapor, *Appl. Phys. Lett.*, vol. 69, pp. 1199-1204 (1996).
- [3] M.T. Turnbull *et al.*: Role of the phase-matching conditions in nondegenerate four-way mixing in hot vapors for the generation of squeezed light, *Phys. Rev. A*, vol. 88, 033845-10 (2013).
- [4] C. F. McCormick *et al.*: Strong relative intensity squeezing by four-wave mixing in rubidium vapor, *Opt. Lett.*, vol. 32, 178-180 (2007).
- [5] J. Okuma *et al.*: Ultraslow matched-pulse propagation in sodium vapor, *Opt. Lett.*, vol. 64, pp. 1654-1656 (2009).

Raman–Ramsey electromagnetically induced transparency in the configuration of counterpropagating pump and probe in vacuum Rb cell

Ivan S. Radojičić,* Milan Radonjić, Marina M. Lekić, Zoran D. Grujić, Dragan Lukić, and Branislav Jelenković

Institute of Physics, University of Belgrade, Pregrevica 118, 11080 Belgrade, Serbia

*Corresponding author: ivan.radojicic@ipb.ac.rs

Received November 19, 2014; revised January 22, 2015; accepted January 22, 2015; posted January 22, 2015 (Doc. ID 226841); published February 13, 2015

Counterpropagating, spatially separated hollow pump and coaxial probe laser beams generate narrow Zeeman electromagnetically induced transparency (EIT) resonances in the vacuum Rb cell. The lasers are locked to D_2 line transition $F_g = 2 \rightarrow F_e = 1$ of ^{87}Rb . For the probe laser beam intensity between 0.1 and 3.0 mW/cm² this Ramsey-type configuration yields dual-structured resonances having a narrow peak on top of a broader pedestal. Linewidths of the narrow peak are nearly independent of the probe laser beam intensity and of the probe diameter (for diameters 0.8 and 2.7 mm), provided that the dark region between the pump and the probe beams is fixed. At the probe laser beam intensities below 0.1 mW/cm² Zeeman EIT is a single narrow resonance. With this geometry of laser beams, and at low probe intensity, the presence of the pump enables the probe EIT, i.e., the probe transmission becomes enhanced in a narrow spectral window. Accompanying theoretical model showed good quantitative agreement with the measurements. © 2015 Optical Society of America

OCIS codes: (270.1670) Coherent optical effects; (300.3700) Linewidth.

<http://dx.doi.org/10.1364/JOSAB.32.000426>

1. INTRODUCTION

Electromagnetically induced transparency (EIT) is a laser(s) transmission peak due to coherences between atomic levels induced by the same laser(s) whose transmission is monitored [1]. EIT as a quantum phenomenon has its classical analog [2]. In a typical interaction scheme, two lasers couple two hyperfine levels (hyperfine coherence) or Zeeman sublevels (Zeeman coherence) with the common excited-state hyperfine level. Hyperfine (Zeeman) level (sublevels) are long lived and degeneracy of the ground-state angular momentum is larger or equal to that of the excited state. Alkali atoms with two long-lived hyperfine levels in the ground state, and optical transitions to excited-state hyperfine level in a suitable wavelength region are most often used in EIT experiments. Quantum EIT, the subject of this investigation, is a manifestation of the coherent superposition of Zeeman sublevels of the ground hyperfine level due to interactions with the laser field. Superposition called dark state [3–5] is decoupled from the interaction and presents foundation of EIT. EIT has gained considerable interest because of nonlinear response and steep dispersion around the atomic resonance at reduced absorption.

A method analog to the Ramsey method of separated oscillatory fields [6] can be utilized for narrowing dark resonances in alkali atoms using thermal atomic beam [7–9] or atoms contained in vacuum glass cells, by spatially separating pump and probe beams [10,11]. Ramsey-like mechanisms yield very narrow EIT resonances in alkali-metal vapor cells with buffer gas (or with antirelaxation wall coating), even with a single laser beam [12,13].

In experiments with vacuum gas cells it is necessary to apply a particular geometry of a hollow pump and a narrow coaxial probe in order to see narrow fringes on the probe EIT [14], or to implement a multizone spectroscopy like in [15]. Instead of spatially separating continuous wave pump and probe, pulses of the pump and probe were used in a Ramsey-like method for narrowing EIT by switching the laser beams on and off. Hyperfine EIT produced in the double Λ scheme with the pump and the weak probe pulse have produced high contrast, very narrow fringes (≈ 100 Hz) in the probe EIT in Cs buffer gas cell [16,17].

In this work we use counterpropagating pump and probe beams to study Ramsey effect on linewidths and amplitudes of the probe Zeeman EIT in Rb vacuum cell. Zeeman coherences are generated in the $F_g = 2$ hyperfine level of the ground state of ^{87}Rb by the pump beam, made in the form of a hollow cylinder. The atomic coherence is carried by the atomic thermal motion to a small-diameter probe beam that passes through the center of the hollow pump laser. There is dark region between the pump and probe beam, which we keep constant in the study. This counterpropagating geometry allows EIT with much weaker probe intensity as opposed to the copropagating pump and probe [14] due to reduced multiple scattering of pump light into the direction of the probe and toward the photodetector. Therefore in this work we cover much lower probe laser beam intensities than in [14]. Also, differently than in [14], here we investigate EIT line shapes for D_2 line of ^{87}Rb . We examine how different probe diameters, for the same dark region, change the shape

of the dual-structured probe EIT resonances having a narrower central peak (due to atomic coherence coming from the pump) and a wider pedestal (due to probe beam influence). The dependence of narrow resonances as a function of the probe laser beam intensity and diameter is studied. Experimental results are compared with the detailed theoretical model based on time-dependent optical Bloch equations (OBEs). We determine the range of the probe intensity when Zeeman EIT has only narrow structure, i.e., the transmission of the probe beam becomes enhanced when the pump is turned on. EIT resonances in vacuum cells, even with the Ramsey method, are wider than EIT in buffer gas cells. However, there is an interest for narrow EIT in vacuum cells at room temperature because atomic collisions, and temperature fluctuations are reduced, which is important for EIT applications.

2. EXPERIMENTAL SETUP

The schematic of the experiment, given in Fig. 1, describes the geometry of laser beams we have used to investigate effects of spatially separating the probe and pump beam on the EIT line shapes. A large-diameter hollow pump beam and narrow coaxial probe beam counterpropagate through the Rb cell. The two beams are generated from the same external cavity diode laser (ECDL). Employing counterpropagating probe and pump beams requires precise laser frequency tuning to the optical transition; otherwise the probe and pump will not be able to interact with the same atoms (atomic velocity is not expected to change in the region between the pump and probe). The laser is locked using the Doppler free dichroic atomic laser lock (DDAVLL) technique [18] on D_2 line transition $F_g = 2 \rightarrow F_e = 1$ of ^{87}Rb , and is linearly polarized. The vacuum Rb cell, 85 mm long and of 25 mm in diameter, is kept at room temperature. The Rb cell is inside cylindrical solenoid that provides longitudinal magnetic field. The triple layers of μ -metal, around the cell, minimize effects of stray magnetic fields. In the experiment we measure the probe transmission as a function of the external magnetic field. Pump intensity is 11.5 mW/cm^2 and the probe intensity varies from 0.1 to 3.0 mW/cm^2 .

We have measured Zeeman EIT by sweeping the magnetic field for two probe $1/e^2$ diameters, 2.7 and 0.8 mm. The pump beam inner diameter is changed from 5 to 7 mm when the probe diameter is changed from 0.8 to 2.7 mm, respectively.

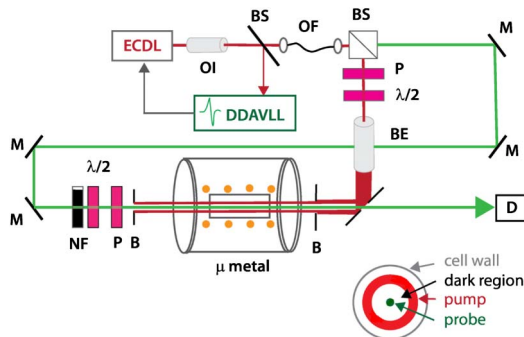


Fig. 1. Experimental setup: ECDL, external cavity diode laser; OI, optical isolator; DDAVLL, Doppler free dichroic atomic laser lock; BS, beam splitter; OF, optical fiber; M, mirrors; P, polarizer; NF, variable neutral density filter; BE, beam expander; $\lambda/2$, retardation plate; B, blade iris diaphragm; D, photodetector.

Thus, the distance between pump and the probe, or “dark region,” is the same and equals 2.1 mm.

3. THEORY

The model is similar to one described in more detail in [19]. The difference stems from the fact that in this case the pump and probe are counterpropagating. The evolution of Rb atoms interacting with spatially separated pump and probe laser beams is described using time-dependent OBEs for the atomic density matrix

$$\frac{d\hat{\rho}}{dt} = -\frac{i}{\hbar}[\hat{H}_{\text{atom}}(B) + \hat{H}_{\text{int}}(t), \hat{\rho}] + \left(\frac{d\hat{\rho}}{dt}\right)_{\text{SE}} + \left(\frac{d\hat{\rho}}{dt}\right)_{\text{relax}}, \quad (1)$$

where

$$\hat{H}_{\text{atom}}(B) = \sum_j \hbar\omega_j(B)|g_j\rangle\langle g_j| + \sum_k \hbar\omega_k(B)|e_k\rangle\langle e_k| \quad (2)$$

is the Hamiltonian of an atom in the external magnetic field \mathbf{B} , aligned with the laser beam propagation direction. Zeeman-shifted energies $\hbar\omega_j(B)$ ($\hbar\omega_k(B)$) correspond to ground (excited) states $|g_j\rangle$ ($|e_k\rangle$). The interaction of an atom with laser is treated in dipole approximation

$$\hat{H}_{\text{int}}(t) = -\sum_{j,k} \mathbf{E}(t) \cdot \mathbf{d}_{jk}(|g_j\rangle\langle e_k| + |e_k\rangle\langle g_j|), \quad (3)$$

where $\mathbf{E}(t)$ is the laser electric field (in the atomic reference frame) and \mathbf{d}_{jk} is the atomic electric dipole moment for the transition between states $|g_j\rangle$ and $|e_k\rangle$. Spontaneous emission is given by

$$\left(\frac{d\hat{\rho}}{dt}\right)_{\text{SE}} = \sum_m 2\hat{\Gamma}_m \hat{\rho} \hat{\Gamma}_m^\dagger - \hat{\Gamma}_m^\dagger \hat{\Gamma}_m \hat{\rho} - \hat{\rho} \hat{\Gamma}_m^\dagger \hat{\Gamma}_m, \quad (4)$$

where $\hat{\Gamma}_m$ are Lindblad operators related to dipole transitions from the excited- to ground-state manifold. In order to obtain good agreement with experimental line shapes, and in addition to [19], we include relaxation of ground-state populations toward the equilibrium

$$\left(\frac{d\hat{\rho}}{dt}\right)_{\text{relax}} = -\gamma \sum_j \left(\rho_{g_j, g_j} - \frac{1 - \pi_e}{8} \right) |g_j\rangle\langle g_j|, \quad (5)$$

where π_e is the total excited-state population. When considering D_2 line transition $F_g = 2 \rightarrow F_e = 1$, the excited hyperfine levels $F_e = 2$ and $F_e = 3$ are also populated due to the Doppler broadening and therefore have to be taken into account. Equations for $F_g = 1$ ground-level density matrix elements are disregarded since that level is not laser-coupled. OBEs are numerically integrated for a collection of atoms passing through the laser beams at different trajectories with velocities sampling Maxwell-Boltzmann distribution. The cylindrical symmetric atomic ensemble density matrix is obtained after averaging over velocities and suitable angular integration. This enables the calculation of atomic vapor polarization, the laser electric field after propagation through the Rb cell and, eventually, Zeeman EIT resonances. Additional details can be found in [20,21].

Pump and probe laser beams have linear polarization and the same frequency. Their propagation directions are

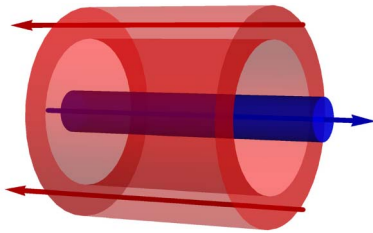


Fig. 2. Radial profiles of counterpropagating hollow pump and coaxial probe laser beams used in the theoretical model.

opposite. As schematically presented in Fig. 2, the probe laser beam passes coaxially through the center of the hollow pump beam. The probe beam profile along radial distance r at the Rb cell entrance is modeled by a Gaussian,

$$I_{\text{probe}}(r) = 2\bar{I}_{\text{probe}} \exp(-2r^2/r_0^2), \quad (6)$$

where r_0 is $1/e^2$ the radius of the probe beam and \bar{I}_{probe} is the probe beam intensity (total probe power divided by $r_0^2\pi$). The pump beam radial intensity profile is taken to be the same along the cell length and ring-shaped:

$$I_{\text{pump}}(r) = \bar{I}_{\text{pump}} a(\text{erf}(p(r-r_1)) - \text{erf}(p(r-r_2))), \quad (7)$$

where \bar{I}_{pump} is the pump beam intensity and a is the normalization constant. Parameter p controls the steepness of the profile near the beam inner and outer edge that are determined by the parameters r_1 and r_2 , respectively.

4. RESULTS AND DISCUSSION

We show results of interactions of the probe beam with atoms prepared in the dark state by the spatially separated pump beam. Both the pump and probe have linear and mutually parallel polarizations. Sweep of the magnetic field provides detuning of two circular components from the two photon resonance among Zeeman sublevels for which $\Delta m_F = 2$. In the following we present EIT line shapes, amplitudes, and linewidths obtained by measuring the probe transmission at different magnetic fields. In this work we are not concerned with absolute values of the probe transmission. Therefore, we present EIT line shapes normalized such that maximal transmission is set to unity.

Figure 3(a) shows measured and Fig. 3(b) calculated Zeeman EIT resonances for two probe laser beam intensities, 0.2 mW/cm^2 (upper rows) and 1.4 mW/cm^2 (lower rows), and two probe laser beam diameters, 0.8 mm (left column) and 2.7 mm (right column). EIT line shapes for both laser beam intensities have dual structure, a narrow peak with fringes appearing on top of a broader pedestal. A broader pedestal is generated by the probe itself, while narrow peak and fringes result from Ramsey interference. Ramsey fringes are well pronounced for the narrower probe beam because of the shorter interaction time of Rb atoms with the probe light, i.e., smaller probe influence. When the probe laser beam intensity is increased, or its diameter is increased, the Ramsey fringes lose their visibility. Theoretical results in Fig. 3(b) are in quite good agreement with the experiment.

EIT widths and amplitudes of the narrow and wide structures are obtained after resolving the two structures in EIT line shapes. Figure 4 presents widths of the narrow structure

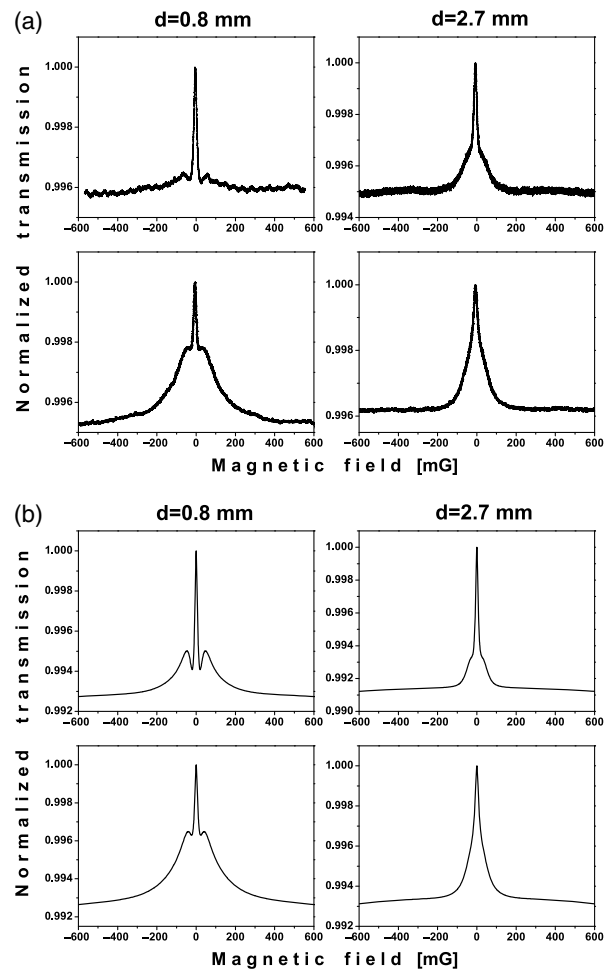


Fig. 3. (a) Experimental and (b) theoretical Zeeman EIT at D_2 line, for two probe laser beam intensities, 0.2 mW/cm^2 (upper rows) and 1.4 mW/cm^2 (lower rows), and two probe laser beam diameters, 0.8 mm (left column) and 2.7 mm (right column).

of EIT resonances, for two probe laser beam diameters. Experimental results are in Fig. 4(a), and theoretical in Fig. 4(b). The linewidth of the narrow structure in our experiment is $\approx 15 \text{ mG}$ or $\approx 18 \text{ kHz}$. This is similar to the narrowest EIT obtained in vacuum alkali gas cells with multizone Ramsey technique [15]. As seen from Fig. 4, the narrow structure EIT linewidth is narrower and also more robust against probe intensity for the narrower probe beam. The behavior of the pedestal width is as expected for a single beam EIT [22]: it is narrower for the wider probe, and it changes much more rapidly with the probe laser beam intensity. Calculated linewidths follow the same trend and the narrower probe beam also gives narrower linewidth.

In the experiment with a single laser beam and coated cell [13], EIT has also dual structure. Similar to our result, narrow structure of EIT in [13] is narrower for the smaller laser beam diameter. Moreover, intensity dependence of the linewidths of the narrower peak is similar as in our setup: EIT linewidth obtained with the narrower beam is less dependent on the laser intensity. Such intensity dependence given in [13] is due to the geometry of the cell and the Ramsey effect of a multiple interaction of atoms with the same laser beam—narrowing the laser increases the dark region, i.e., time that the atom spends in the dark. The similar behavior of the

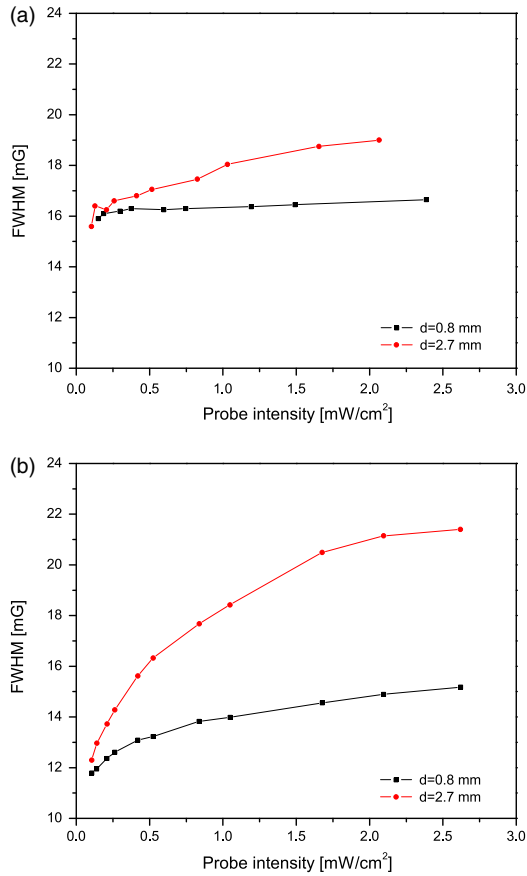


Fig. 4. (a) Experimental and (b) theoretical full width at half maximum of the narrow structure of EIT as a function of the probe laser beam intensity, for two probe laser beam diameters, 0.8 and 2.7 mm.

narrow peak of the EIT in our work has a different explanation. The probe laser beam, apart from probing the atoms coherently prepared in the pump beam, influences the atomic evolution, which affects the narrow structure linewidth. During atomic passage through the laser beams the atomic state changes due to competitive effects of the laser electric field and the external magnetic field. The laser field continuously prepares the atoms into the dark state. The external magnetic field causes oscillations of the atomic ground-state coherences at the corresponding Larmor frequency and alters the atoms from the dark state. When the external magnetic field is zero the atoms reach the dark state inside the strong pump beam, which consequently leads to a maximum in the probe transmission. At nonzero magnetic field the state of the atoms passing through the probe beam differs from the dark state, so that the probe transmission decreases. However, this decrease in probe transmission due to the influence of the magnetic field is partially compensated by preparation of the atoms into the dark state within the probe beam. Hence, the actual probe transmission at some magnetic field is somewhat larger than the one expected without the probe influence. This causes broadening of the narrow structure in Zeeman EIT resonances that becomes more pronounced as the probe intensity and/or diameter increases.

Figure 5 shows measured and calculated amplitudes of the narrow structure of EIT resonances, for probe laser beam diameters 0.8 mm [Fig. 5(a)] and 2.6 mm [Fig. 5(b)]. As both

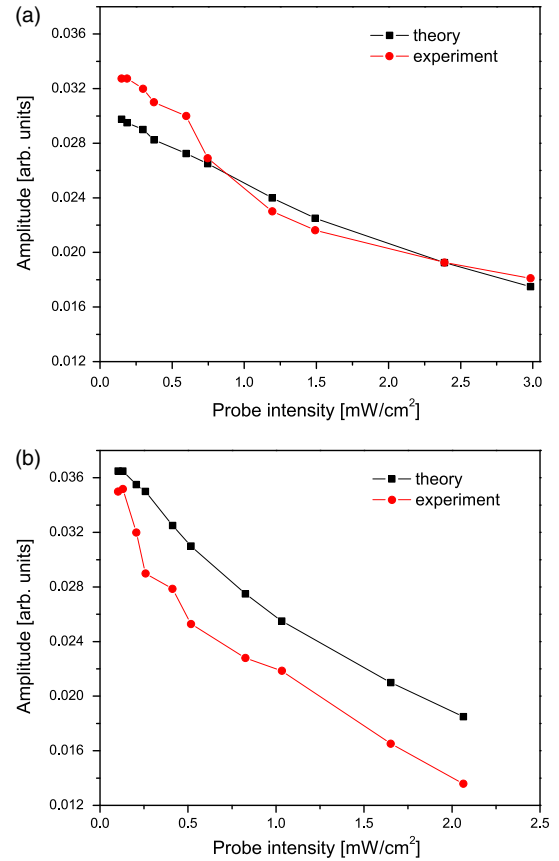


Fig. 5. Experimental and theoretical results for the amplitudes of the narrow structure of EIT resonances for two probe laser beam diameters: (a) 0.8 mm and (b) 2.7 mm.

experiment and theory show, amplitudes of narrow peaks of the probe EIT are nearly independent on probe beam diameter. Their dependence on the probe intensity and diameter is different than the amplitude of the wide structure EIT.

Amplitudes of the narrow peak of the probe EIT (obtained when the pump laser beam is turned on) have different dependence on the probe laser beam intensity than a single beam EIT, tuned to the same Raman resonance and with the same diameter. This is demonstrated in Fig. 6 where we plot amplitudes of both narrow and wide structure as a

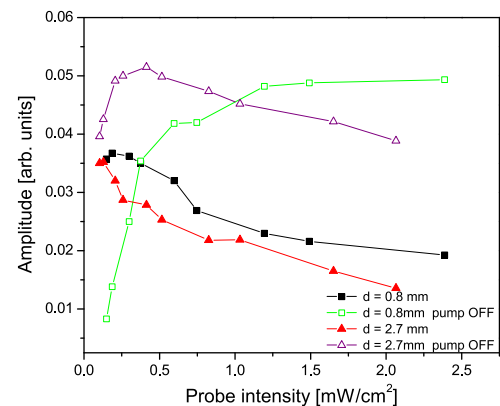


Fig. 6. Amplitudes of the probe EIT with and without pump laser beam, for two probe laser beam diameters: 0.8 and 2.7 mm. Amplitudes of wide (narrow) structures are shown for the pump laser beam turned off (on).

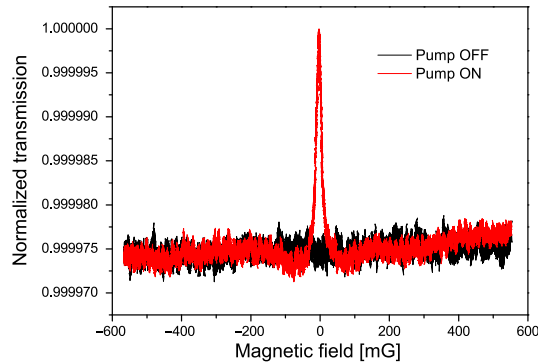


Fig. 7. Probe beam Zeeman EIT at D_2 line, with and without the pump beam. Intensities of the probe and pump beams are 0.1 mW/cm^2 and 11.5 mW/cm^2 , respectively.

function of probe intensity, for two probe diameters. The maximum of the narrow structure of the probe EIT in the Raman–Ramsey configuration is at very low laser intensities, below values that we can detect in the experiment.

At very low probe laser beam intensities, below 0.1 mW/cm^2 , the probe EIT has only narrow structure. The transmission of the weak probe can be controlled in a narrow spectral range around zero magnetic field by switching the pump beam on/off. For small magnetic fields and when the pump laser beam is present, the atoms coming into the probe beam are already coherently prepared into the dark state. This leads to the increase of the probe transmission, as presented in Fig. 7, where we show probe EIT for 0.8 mm probe beam diameter and for probe beam intensity of 0.1 mW/cm^2 , without or with pump beam of intensity 11.5 mW/cm^2 . Enhancement of the probe transmission is better for larger pump beam intensities.

5. CONCLUSION

We presented effects of the counterpropagating spatially separated pump and probe laser beam configuration on the probe Zeeman EIT. Both pump and probe beams are tuned to the D_2 line of ^{87}Rb . For the geometry of the experiment, with the probe coaxial with the surrounding hollow pump and small dark region between the pump and probe, we showed that in the vacuum cell, like in cells with antirelaxation coating, resonances can be narrower when the probe diameter is smaller. For the probe of 0.8 mm in diameter we observed and calculated narrower linewidths, almost independent of the probe laser beam intensity. Also, for this small probe diameter, when its intensity is below 0.1 mW/cm^2 , dual structure of Zeeman EIT turns in to a single narrow EIT. Probe transmission is enhanced in a narrow range of small magnetic fields when the pump laser beam is present, which is akin to optical switch behavior.

ACKNOWLEDGMENTS

This work was supported by the Ministry of Education and Science of Serbia, under grants III45016 and OI171038, and also by SCOPES JRP IZ73Z0_127942.

REFERENCES

- S. E. Harris, "Electromagnetically induced transparency," *Phys. Today* **50**(7), 36–42 (1997).
- C. L. Garrido Alzar, M. A. G. Martinez, and P. Nussenzeig, "Classical analog of electromagnetically induced transparency," *Am. J. Phys.* **70**, 37–42 (2002).
- G. Alzetta, A. Gozzini, L. Moi, and G. Orriols, "An experimental method for the observation of r.f. transitions and laser beat resonances in oriented Na vapour," *Nuovo Cimento B* **36**, 5–20 (1976).
- E. Arimondo and G. Orriols, "Nonabsorbing atomic coherences by coherent two-photon transitions in a three-level optical pumping," *Lett. Nuovo Cimento Soc. Ital. Fis.* **17**, 333–338 (1976).
- F. Renzoni, W. Maichen, L. Windholz, and E. Arimondo, "Coherent population trapping with losses observed on the Hanle effect of the D_1 sodium line," *Phys. Rev. A* **55**, 3710–3718 (1997).
- N. F. Ramsey, *Molecular Beams* (Oxford University, 1956).
- B. Schuh, S. I. Kanorsky, A. Weis, and T. W. Hänsch, "Observation of Ramsey fringes in nonlinear Faraday rotation," *Opt. Commun.* **100**, 451–455 (1993).
- J. E. Thomas, P. R. Hemmer, S. Ezekiel, C. C. Leiby, Jr., R. H. Picard, and C. R. Willis, "Observation of Ramsey fringes using a stimulated, resonance Raman transition in a sodium atomic beam," *Phys. Rev. Lett.* **48**, 867–870 (1982).
- G. Theobald, V. Giordano, N. Dimatcq, and P. Cerez, "Observation of narrow Ramsey-type resonances in a caesium beam due to Zeeman coherences," *J. Phys. B* **24**, 2957–2966 (1991).
- S. Nakayama, G. W. Series, and W. Gawlik, "Larmor precession in polarization spectroscopy with spatially separated beams," *Opt. Commun.* **34**, 389–392 (1980).
- A. S. Zibrov and A. B. Matsko, "Optical Ramsey fringes induced by Zeeman coherence," *Phys. Rev. A* **65**, 013814 (2001).
- Y. Xiao, I. Novikova, D. F. Phillips, and R. L. Walsworth, "Diffusion-induced Ramsey narrowing," *Phys. Rev. Lett.* **96**, 043601 (2006).
- M. Klein, M. Hohensee, D. F. Phillips, and R. L. Walsworth, "Electromagnetically induced transparency in paraffin-coated vapor cells," *Phys. Rev. A* **83**, 013826 (2011).
- Z. D. Grujić, M. Mijailović, D. Arsenović, A. Kovačević, M. Nikolić, and B. M. Jelenković, "Dark Raman resonances due to Ramsey interference in vacuum vapor cells," *Phys. Rev. A* **78**, 063816 (2008).
- H. Failache, L. Lenci, and A. Lezama, "Raman-Ramsey multizone spectroscopy in a pure rubidium vapor cell," *Phys. Rev. A* **81**, 023801 (2010).
- T. Zanon, S. Guerandel, E. de Clercq, D. Holleville, N. Dimarcq, and A. Clairon, "High contrast Ramsey fringes with coherent-population-trapping pulses in a double lambda atomic system," *Phys. Rev. Lett.* **94**, 193002 (2005).
- X. Liu, J.-M. Mérola, S. Guérandel, E. de Clercq, and R. Boudot, "Ramsey spectroscopy of high-contrast CPT resonances with push-pull optical pumping in Cs vapor," *Opt. Express* **21**, 12451 (2013).
- K. L. Corwin, Z. Lu, C. F. Hand, R. J. Epstein, and C. E. Wieman, "Frequency-stabilized diode laser with the Zeeman shift in an atomic vapor," *Appl. Opt.* **37**, 3295–3298 (1998).
- Z. D. Grujić, M. Lekić, M. Radonjić, D. Arsenović, and B. M. Jelenković, "Ramsey effects in coherent resonances at closed transition $F_g = 2 \rightarrow F_e = 3$ of ^{87}Rb ," *J. Phys. B* **45**, 245502 (2012).
- M. Radonjić, D. Arsenović, Z. Grujić, and B. M. Jelenković, "Coherent population trapping linewidths for open transitions: cases of different transverse laser intensity distribution," *Phys. Rev. A* **79**, 023805 (2009).
- A. J. Krmpot, M. Radonjić, S. M. Ćuk, S. N. Nikolić, Z. D. Grujić, and B. M. Jelenković, "Evolution of dark state of an open atomic system in constant intensity laser field," *Phys. Rev. A* **84**, 043844 (2011).
- E. Figueroa, F. Vewinger, J. Appel, and A. I. Lvovsky, "Decoherence of electromagnetically induced transparency in atomic vapor," *Opt. Lett.* **31**, 2625–2627 (2006).



Република Србија
Универзитет у Београду
Физички факултет
Д.Бр.2011/8006
Датум: 18.01.2018. године

На основу члана 161 Закона о општем управном поступку и службене евиденције издаје се

УВЕРЕЊЕ

Радојичић (Слободан) Иван, бр. индекса 2011/8006, рођен 09.07.1980. године, Чачак, Чачак-град, Република Србија, уписан школске 2017/2018. године, у статусу: самофинансирање; тип студија: докторске академске студије; студијски програм: Физика.

Према Статуту факултета студије трају (број година): три.
Рок за завршетак студија: у двоструком трајању студија.

Ово се уверење може употребити за регулисање војне обавезе, издавање визе, права на дечији додаток, породичне пензије, инвалидског додатка, добијања здравствене књижице, легитимације за повлашћену возњу и стипендије.



Овлашћено лице факултета

[Handwritten signature]

РЕПУБЛИКА СРБИЈА



ФИЗИЧКИ ФАКУЛТЕТ
УНИВЕРЗИТЕТА У БЕОГРАДУ

ДИПЛОМА

О СТЕЧЕНОМ ВИСОКОМ ОБРАЗОВАЊУ

Радошчић Слободана Иван

РОЂЕН-А 9-III-1980. ГОДИНЕ У ЧАЧКУ, ЧАЧАК
СТРАНА , УПИСАН-А 1999/2000. ГОДИНЕ,
А ДАНА 5. НОВЕМБРА 2010. ГОДИНЕ, ЗАВРШИО-ЛА ЈЕ СТУДИЈЕ НА
ФИЗИЧКОМ ФАКУЛТЕТУ УНИВЕРЗИТЕТА У БЕОГРАДУ, НА
СТУДИЈСКОЈ ГРУПИ ФИЗИКА
СА ОПШТИМ УСПЕХОМ 8,68 (осам и 68/100) У ТОКУ СТУДИЈА И
ОЦЕНОМ 10 (десет) НА ДИПЛОМСКОМ ИСПИТУ.

НА ОСНОВУ ТОГА ИЗДАЈЕ МУ-ЈОЈ СЕ ОВА ДИПЛОМА О СТЕЧЕНОМ ВИСОКОМ
ОБРАЗОВАЊУ И СТРУЧНОМ НАЗИВУ

ДИПЛОМИРАНИ ФИЗИКАР ЗА ПРИМЕНЉУ ФИЗИКУ И ИНФОРМАТИКУ

РЕДНИ БРОЈ ИЗ ЕВИДЕНЦИЈЕ О ИЗДАТИМ ДИПЛОМАМА 21052010

У БЕОГРАДУ, 5. НОВЕМБРА 2010.

ГОДИНЕ

ДЕКАН

проф. др. Јулијана Јековић

РЕКТОР

проф. др. Франко Чолаковић